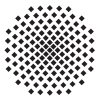

Universität Stuttgart

INSTITUT FÜR MECHANIK

Quantification of Guided Wave Mode Conversion at Free Edge in Cylindrical Structures using BEM

by
Anuj Sharma

Master Thesis

Guided by
Dipl.-Ing. Stefan Bischoff

Institut for Applied and Experimental Mechanics
Universitaet Stuttgart
o. Prof. Dr.-Ing. habil. L. Gaul
Prof. Dr.-Ing. A. Kistner

June 2011

Contents

List of Figures

1 Introduction

1.1 Motivation

The Electric Transmission lines used to transmit power from power station to other units, are prone to damage due to various conditions. Some of reasons could be identified as the weather conditions pertaining to rain which causes corrosion, windy loads causing vibrations, temperature effects etc, which are prone to causes damages. The damages of these high transmission lines are quiet dangerous, as it carries high voltage and could cause casualties with loss of power transmission to important sectors. Hence a proper and regular monitoring system needed as these lines are installed for long use. One of damages presented is related to generation of crack and crack propagation.The conventional methods have been on lines of visual inspection which include high amount risk and very expensive. This demands for the need to have better experimental and simulations methods to overcome the problems and avoid casualties with measurements done from distance far from the transmission lines. One method that could be realized is non destructive testing method using ultrasonic waves.

The simulation in past and present have been modeled through the methods like Modal Decomposition method and Finite element method. These methods gets complicated for crack having other than vertical cross-section. The Boundary Element method can yield results for different cross sectional cracks with less time invested in the computation. The work in this thesis concentrates on analysis of mode conversions at free edge.

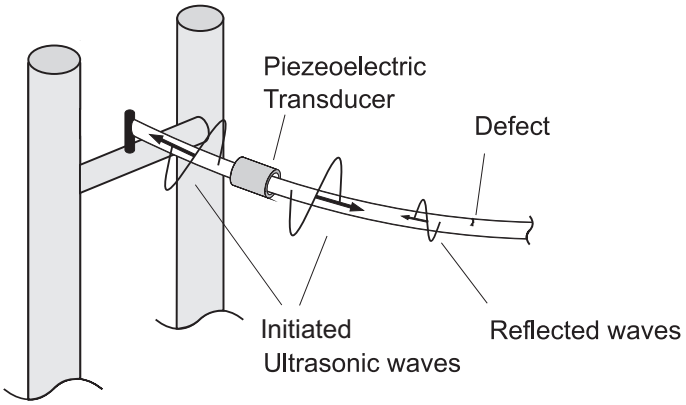

Figure 1.1: Damage detection in transmission lines by wave propagation.

1.2 Introduction

Mode conversion occurs when an incident wave for example longitudinal wave hits surface at discontinuities. The work presented here is to study the mode conversion behavior at free edge of a cylinder using Boundary Element method. For the free edge, all the incident wave gets completely reflected back, and to study the behavior of same superposition of waves done of both incident and reflected waves. The choice of waves used have been Guided waves due to their advantage of long distance propagation and are weakly attenuated.

The modal decomposition method is quiet robust for vertical cracks but as the crack geometry gets complicated, the modes available for the constant cross section at initial can't be used. In the following boundary element method is formulated in conjunction with modal decomposition method to analyze the wave propagation and mode conversion in structures. The analysis on semi infinite cylindrical structure being case of interest. The region near the free edge is modeled using surface 2D elements, while the rest of the structure is modeled using volume 3D elements. A FE based method developed from [Mace et al.] is applied to get all possible wave modes and wave numbers, respectively. The obtained results could be integrated to the left and right cross-sectional boundaries of the boundary element modeled waveguide cross-section.

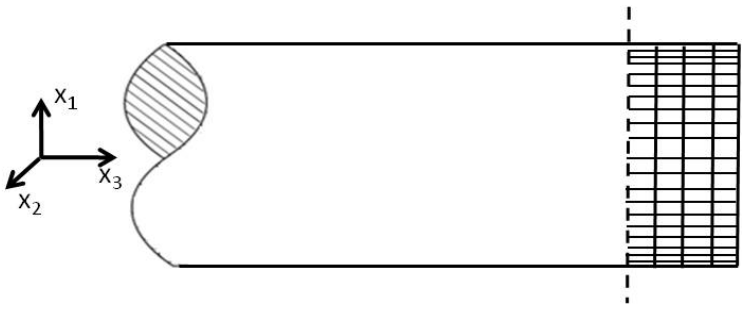

Figure 1.2: Boundary elements near free edge region

The elastodynamic behavior of the discretized waveguide is described by the basic boundary integral equation [Gaul et al.], which could be formulated in matrix form as

$$\boldsymbol{H}\ \boldsymbol{u} = \boldsymbol{G}\ \boldsymbol{q} \tag{1.1}$$

where, $\boldsymbol{H}$ and $\mathbf{G}$ matrices represents the contributions of the traction and displacements fields respectively on the boundary of the domain and $\boldsymbol{u}$ and $\boldsymbol{q}$ are the unknown displacement and traction fields. Now, above equation holds true for any geometry, such that changes in geometry of the domain brings changes only to the $\boldsymbol{H}$ and $\boldsymbol{G}$ matrices. Hence, the method is suitable for any types of discontinuities. Also, the method is better for secondary field variable results also. Due to reduction in the order of elements used in boundary elements, the time consumption for computations for complicated geometries involving discontinuities is less

compared to finite element method. The boundary conditions associated with the traction free circumferential surface and free edge surface, enable to set the nodal traction on the respective surfaces to zero. Also, the relations of displacement and tractions at the left and right cross-sectional boundaries of the waveguide are known. The system of equation could solved as

$$\boldsymbol{A}\ \boldsymbol{y} = \boldsymbol{F} \tag{1.2}$$

where, $\boldsymbol{y}$ contains all the unknown variables. The main task is to estimate the reflection coefficients, which accounts for the relation between the intensity of reflected waves with incident waves, at spectrum of frequencies which can give notions about the different modes generated with increase in frequency. Each propagating mode obtained in reflection coefficient over different frequencies follow the continuity and conservation of energy principles at each individual frequency.

2 Guided Waves in Cylindrical structures

2.1 Wave Guide

Disturbances in infinite or semi-infinite media, usually only have a significant effect within relatively small depths. This could be explained as when in free space the waves travel as a spherical wave in all directions, due to which the power loss increases squarely with respective to distance from source. This fact significantly limits the range in which the body waves can be used for crack detection. Hence required to confine the propagation in one direction to reduce the loss.

Previous experiment results enable that in a cylindrical rod, a disturbance is reflected at the surface of the rod with less attenuation due to geometrical effects. These structure which allow waves to travel long distances with weak attenuation are referred as Wave Guides. The confinement of waves inside the waveguide are associated with the multiple reflections from the boundaries as shown in figure 2.1. Due to large distance travel, it justifies the use of elastic waves for damage detection. The Guided waves are the ultrasonic waves that are similar to Rayleigh

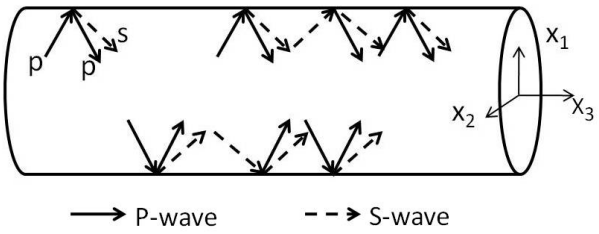

Figure 2.1: Multiple internal reflections in cylindrical waveguide

and lamb waves, whose velocity is not only dependent on the material properties but also onto the thickness of the material and frequency.
For one dimensional axial wave propagation, the partial differential equation is [see Achenbach [1]]

$$\frac{\partial^2 u_z}{\partial z^2} = \frac{\rho}{E}\frac{\partial^2 u_z}{\partial t^2}. \tag{2.1}$$

But the equation 2.1 couldn't be applicable for higher frequencies as there results don't agree with experiments ones. To a solution more applicable, dispersive behavior of the waves needed to be taken into account. Here, we would assume

harmonic solutions for longitudinal and lateral components to satisfy the governing equation of wave propagation, the Lamé- Navier equation

$$(\lambda + \mu)u_{j,ij} + \mu u_{i,jj} + \rho b_i = \rho u_i, \tag{2.2}$$

which is satisfied by displacement fields of the form

$$u_i = \hat{u}_i e^{(k_i x_i - \omega t)}. \tag{2.3}$$

The above for cylindrical wave guide could be expressed as

$$\boldsymbol{u}(x,t) = \hat{\boldsymbol{u}}(x_1, x_2)e^{i(kx_3 - \omega t)} \tag{2.4}$$

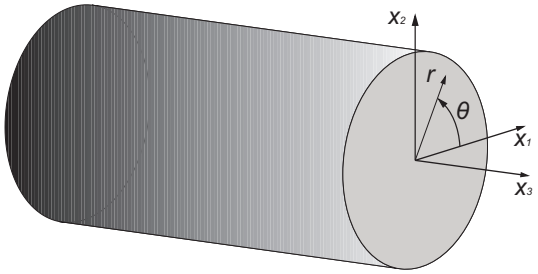

Figure 2.2: cylinder in polar and cartesian coordinates

Using the Helmholtz decomposition $\boldsymbol{u} = \nabla\phi + \nabla \times \psi$, the harmonic solutions of same need to satisfy the boundary conditions. For the completeness of solution, decoupling condition $\nabla.\psi = 0$ is utilized. With example of traction free cylinder, makes the stresses on boundaries to zero. Also the relations between stress, strain and displacement available from Hooke's law and constitutive laws. The harmonic solution assumption could be reduced with consideration of flexural, torsional and longitudinal modes on scalar and vector potential ϕ and H respectively to

$$\begin{aligned}
\phi &= AJ_n(\alpha r)\cos n\theta e^{i(kx_3 - \omega t)} && (2.5)\\
H_z &= BJ_n(\beta r)\sin n\theta e^{i(\xi z - \omega t)} && (2.6)\\
H_\theta &= -CJ_{n+1}(\beta r)\cos n\theta e^{i(\xi z - \omega t)} && (2.7)\\
H_r &= CJ_{n+1}(\beta r)\sin n\theta e^{i(\xi z - \omega t)}.
\end{aligned}$$

where

$$\alpha^2 = \frac{\omega^2}{c_L^2} - k^2 \quad \text{and} \quad \beta^2 = \frac{\omega^2}{c_T^2} - k^2 \tag{2.8}$$

The coefficients c_L and c_T are the longitudinal and transverse wave speed, which depend on the material parameters λ and μ.

$$c_L = \sqrt{\frac{(\lambda + 2\mu)}{\rho}} \quad , \quad c_T = \sqrt{\frac{\mu}{\rho}}. \tag{2.9}$$

where the two lamé constants λ and μ could be associated with the known material parameters like Young's modulus (E), shear modulus (G) and Poisson's ratio (ν), such that

$$\mu = \frac{E}{2(1+\nu)} \qquad \lambda = \frac{E\nu}{(1+\nu)(1-2\nu)}. \tag{2.10}$$

More complicated differential equations for the other coefficients exists [see Graff [6]]. All the solutions are replaced into displacement assumptions from Helmholtz decomposition. The same are then substituted into stress on surface from the constitutive law. When subjected to boundary conditions,

$$\sigma_{rr} = \sigma_{r\theta} = \sigma_{rz} = 0, \tag{2.11}$$

the system of equations containing the coefficients makes the determinant equal to zero and giving the general frequency equation. The determinant specifies the frequency equation for all modes.

2.2 Dispersion Curves

Extraction of roots of frequency equation would yield solutions for phase velocity versus frequency or frequency times thickness. These plots shows how phase velocity changes with respect to frequency giving the idea about the stretch or dispersive behavior while wave propagation. Similarly, the plot between wave number and frequency could also be obtained as wave number represented in terms of velocity and frequency. An example of same for longitudinal wave known as Pochhammer-Chree frequency equation is presented as

$$\frac{2\alpha}{a}(\beta^2+k^2)J_1(\alpha a)J_1(\beta a) - (\beta^2-k^2)^2 J_0(\alpha a)J_1(\beta a) - 4k^2\alpha\beta J_1(\alpha a)J_0(\beta a) = 0 \tag{2.12}$$

A dispersion curve for a cylindrical rod with radius a =2 mm and steel material parameters have been shown in figure 2.3.

In following analysis, damping is neglected hence wave numbers have purely real part.

$$\begin{aligned} \text{Material Density} &: 2700\ kg/m^3 \\ \text{Young's Moduls} &: 210\ GPa \\ \text{Poissons ratio} &: 0.25 \end{aligned} \tag{2.13}$$

The individual modes could be obtained from the choice of order of the Bessel function used in frequency equation. Longitudinal modes are characterized such that the displacement and stress fields are independent of the coordinate θ and rotational symmetry in the axial direction. For this, condition is $n = 0$. The displacement fields for the cylinder has been shown in figure 2.4. It could be

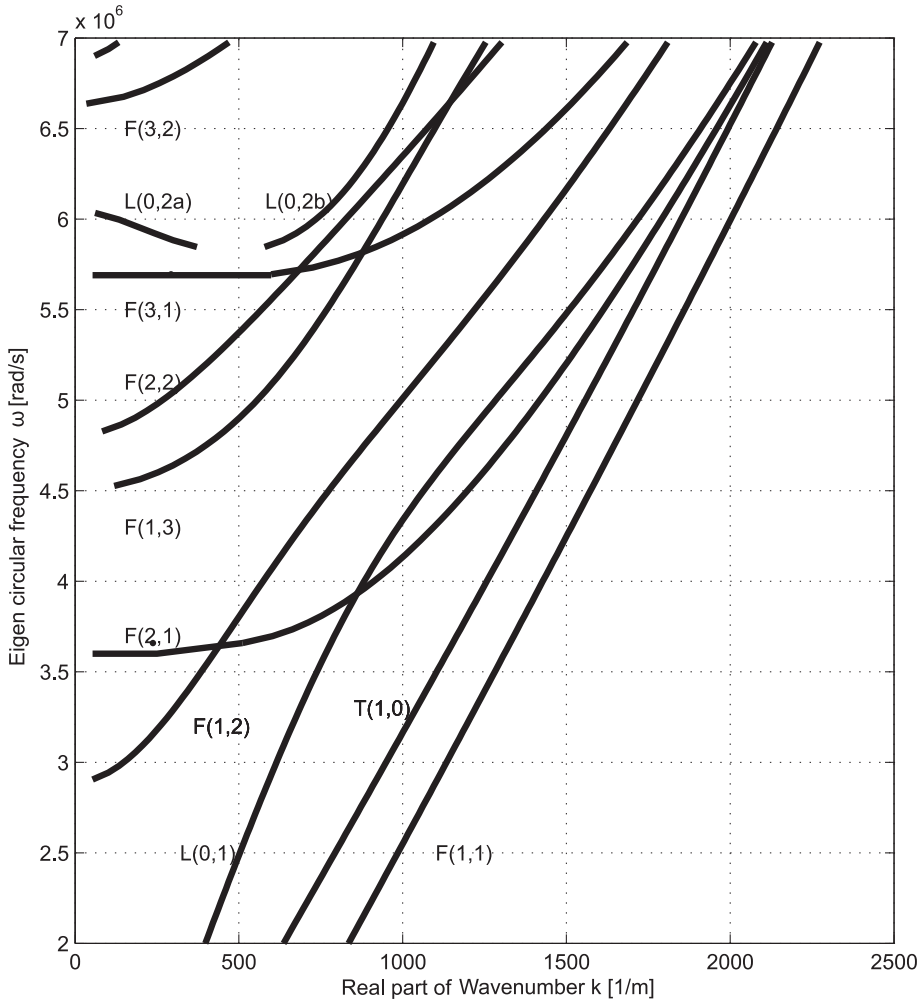

Figure 2.3: Dispersion curve

seen in figure 2.4 that the longitudinal mode has displacement only in axial and radial components as these are independent of θ and the tangential displacement is zero. The same when extended to flexural mode, the condition for the same is that the order of Bessel function $n \geq 1$. The flexural mode is dependent on the circumferential angle unlike longitudinal mode. The frequency equation is obtained similarly by replacing the displacements into stresses expressions on traction free surface with $r = a$, obtained are three homogeneous equations and equating determinant to zero yields frequency equation. The displacement fields in the axial, radial and tangential directions are shown in Figure 2.5. The current order$n = 1$, the tangential displacement profile of the edge nodes are removed by dividing the number of extrema. Here, the existence of two extreme points leads to a nodal line through the cylinder cross section, allowing the nodes of any shifts and hence no vibration.

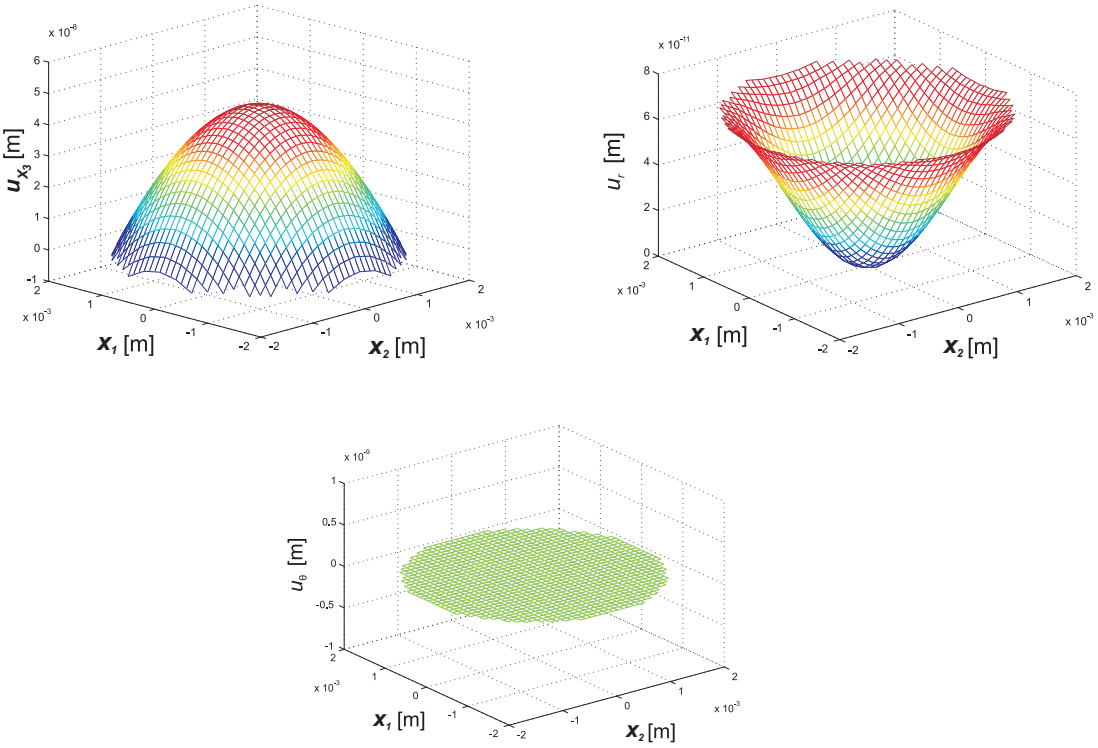

Figure 2.4: a) axial displacement b) radial displacement c)tangential displacement of traction free cylinder for longitudinal mode

2.3 Waveguide-FE Method

The dynamic behavior of structure could be analyzed using the Waveguide finite element method. The method transforms the dynamic stiffness matrix containing the mass and stiffness matrix into transfer matrix. The solution of transfer matrix is obtained in form of eigenvalues and eigenvectors which represent wave number and wave modes respectively. The equation of motion for a waveguide structure is expressed as

$$\boldsymbol{M}\ddot{\boldsymbol{u}} + \boldsymbol{C}\dot{\boldsymbol{u}} + \boldsymbol{K}\boldsymbol{u} = \boldsymbol{F} \tag{2.14}$$

where, $\boldsymbol{M}$ represents the mass matrix, $\boldsymbol{C}$ damping matrix, $\boldsymbol{K}$ stiffness matrix, $\boldsymbol{u}$ unknown nodal displacement vector and $\boldsymbol{F}$ the load vector. The harmonic time equation of motion in explicit form is represented as

$$(-\omega^2\boldsymbol{M} + i\omega\boldsymbol{C} + \boldsymbol{K})\hat{\boldsymbol{u}} = \hat{\boldsymbol{F}} \tag{2.15}$$

The equation above could be expressed as

$$\tilde{\boldsymbol{D}}\hat{\boldsymbol{u}} = \hat{\boldsymbol{F}} \tag{2.16}$$

where, $\tilde{\boldsymbol{D}}$ is referred as dynamic stiffness. The above could be rearranged in with respect to unknown displacements and forces on right, left and interior nodes as shown in figure 2.6.

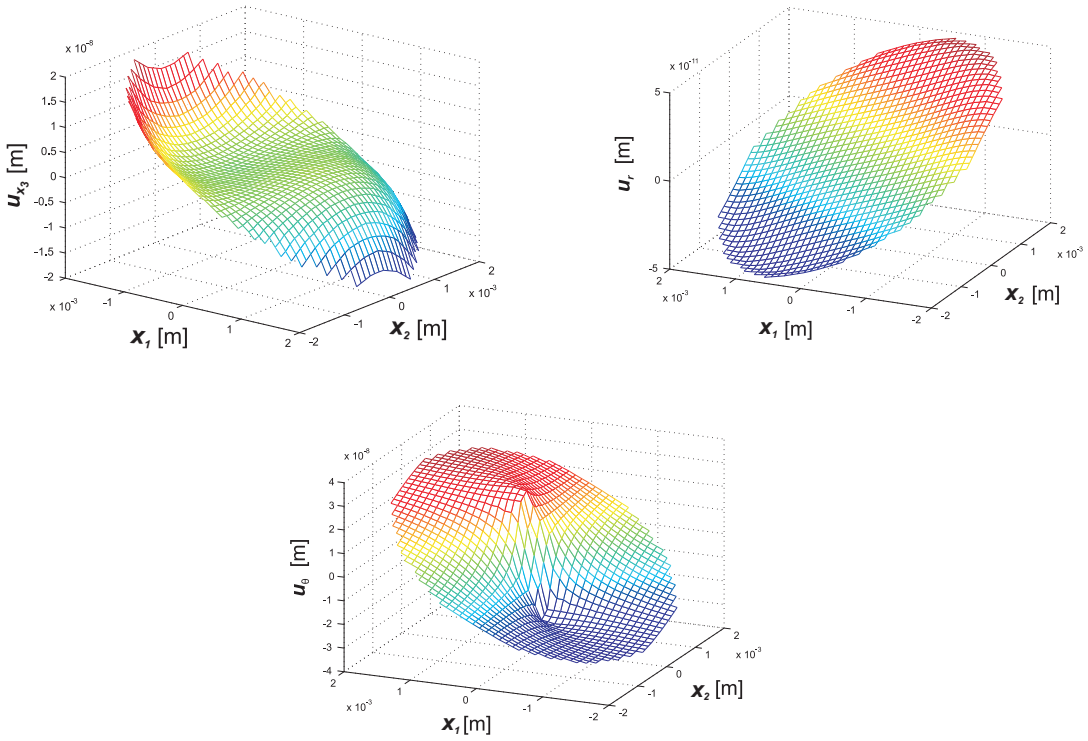

Figure 2.5: a) axial displacement b) radial displacement c)tangential displacement of traction free cylinder for flexural mode with n=1

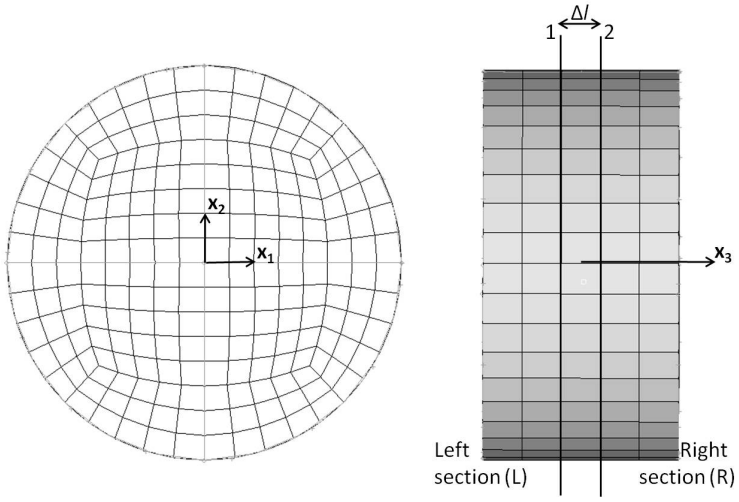

Figure 2.6: Fine discretization of cylinder into left and right segments

While no applied forces forces on interior, the system would be reduced inclusive with the terms associated with interiors nodes also, as represented below,

$$\begin{bmatrix} \boldsymbol{D}_{LL} & \boldsymbol{D}_{LR} \\ \boldsymbol{D}_{RL} & \boldsymbol{D}_{RR} \end{bmatrix} \begin{bmatrix} \boldsymbol{u}_L \\ \boldsymbol{u}_R \end{bmatrix} = \begin{bmatrix} \boldsymbol{F}_L \\ \boldsymbol{F}_R \end{bmatrix} \tag{2.17}$$

For symmetric mass, stiffness and damping matrices, the dynamic stiffness matrix

is also symmetric. For no external forces applied, the continuity of displacements and equilibrium of forces at two different cross-sections namely (1) and (2) are used as

$$\boldsymbol{u}_L^{(2)} = \boldsymbol{u}_R^{(1)} \qquad \boldsymbol{F}_L^{(2)} + \boldsymbol{F}_R^{(1)} = 0. \tag{2.18}$$

The above represented with help of Transfer matrix as

$$\begin{bmatrix} \boldsymbol{u}_L^{(2)} \\ \boldsymbol{F}_L^{(2)} \end{bmatrix} = \boldsymbol{T} \begin{bmatrix} \boldsymbol{u}_R^{(2)} \\ \boldsymbol{F}_R^{(2)} \end{bmatrix} \tag{2.19}$$

where $\boldsymbol{T}$ Transfer matrix depending only on dynamic stiffness matrices is expressed as

$$\boldsymbol{T} = \begin{bmatrix} -\boldsymbol{D}_{LR}^{-1}\boldsymbol{D}_{LL} & \boldsymbol{D}_{LR}^{-1} \\ -\boldsymbol{D}_{RL} + \boldsymbol{D}_{RR}\boldsymbol{D}_{LR}^{-1}\boldsymbol{D}_{LL} & -\boldsymbol{D}_{RR}\boldsymbol{D}_{LR}^{-1} \end{bmatrix} \tag{2.20}$$

The wave propagation is represented by the above transfer matrix, and solving for the eigenvalues and vectors are means to represent wave numbers and mode shapes. Considering the free wave propagation, the successive displacements and forces are represented as

$$\begin{bmatrix} \boldsymbol{u}_L^{(2)} \\ \boldsymbol{F}_L^{(2)} \end{bmatrix} = \lambda_{\mathbf{e}} \begin{bmatrix} \boldsymbol{u}_R^{(2)} \\ \boldsymbol{F}_R^{(2)} \end{bmatrix} \tag{2.21}$$

The factor $\lambda_{\mathbf{e}} = e^{ik\Delta l}$ could be replaced, with Δl being the thickness as shown in figure 2.6. Hence above could be transformed into a form using equation 2.19 as

$$\boldsymbol{T} \begin{bmatrix} \boldsymbol{u}_R^{(2)} \\ \boldsymbol{F}_R^{(2)} \end{bmatrix} = e^{ik\Delta l} \begin{bmatrix} \boldsymbol{u}_R^{(2)} \\ \boldsymbol{F}_R^{(2)} \end{bmatrix} \tag{2.22}$$

Although the above equation represents the basic principle of waveguide FEM, but require numerical treatment due to ill conditioned eigenvalues. Once known the eigenvalues and vectors, this could be utilized for representation of displacement field of the waveguide structure.

3 Theory and Formulation

3.1 Governing Equations for 3D Elastodynamics

3.1.1 Formulation of field equations

The constitutive law relating the stresses with strains could be used to obtain the field equation of elastodynamics.

$$\sigma_{ij} = \lambda\ \delta_{ij}\ \epsilon_{kk} + 2\mu\ \epsilon_{kk}, \tag{3.1}$$

where, σ and ϵ are symmetric stress and strain tensors respectively, with small strain deformation tensor defined as

$$\epsilon_{ij} = \frac{1}{2}(u_{i,j} + u_{j,i}). \tag{3.2}$$

The equilibrium equation is presented below,

$$\sigma_{ij,j}\ + \rho b_i = \rho \ddot{u}_i. \tag{3.3}$$

With substitution of equation 3.1in above results in the required field equation, we obtain

$$(\lambda + \mu)u_{j,ij} + \mu u_{i,jj} + \rho b_i = \rho u_i. \tag{3.4}$$

$$(\lambda + \mu)\nabla(\nabla.\boldsymbol{u}) + \mu\nabla^2\boldsymbol{u} + \rho\boldsymbol{b} = \rho\ddot{\boldsymbol{u}}. \tag{3.5}$$

The equation is also famously known as Lame' navier equation. Using the vector identity $\nabla^2\boldsymbol{u} = \nabla(\nabla.\boldsymbol{u}) - \nabla \times \nabla \times \boldsymbol{u}$, the equation obtained is

$$(\lambda + 2\mu)\nabla(\nabla.\boldsymbol{u}) - \mu\nabla \times \nabla \times \boldsymbol{u} + \rho\boldsymbol{b} = \rho\ddot{\boldsymbol{u}}. \tag{3.6}$$

Introducing the two constants associated with the material parameters, $c_1^2 = \dfrac{(\lambda + 2\mu)}{\rho}$ and $c_2^2 = \dfrac{\mu}{\rho}$, the field equation 3.5 could be represented as

$$(c_1^2 - c_2^2)\nabla(\nabla.\boldsymbol{u}) + c_2^2\nabla^2\boldsymbol{u} + \boldsymbol{b} = \ddot{\boldsymbol{u}}. \tag{3.7}$$

The previous equation would be used in later sections for the derivation of fundamental solution. The two constants $\boldsymbol{c}_1$ and $\boldsymbol{c}_2$ are related to wave velocities, which are explained in coming steps. The Navier equation could be transformed

into the elastodynamic wave equation by using the Helmholtz decomposition of the displacement vector field vector into its rotational and solenoidal part.

$$\boldsymbol{u} = \nabla\phi + \nabla \times \psi, \tag{3.8}$$

with $\nabla \times (\nabla\phi) = 0$ and $\nabla.(\nabla \times \psi) = 0$ taken into consideration. Here ϕ and ψ are the scalar and vector potentials respectively. The Helmholtz decomposition could be utilized for any piecewise differentiable vector with consideration that it decreases to zero with an order of r^{-2}, when at large distances r from the origin. For the completeness of the solution of the displacement vector, a condition for decoupling between the three terms associated with vector potential and one term of scalar potential is utilized as

$$\nabla.\psi = 0. \tag{3.9}$$

Hence the field equation 3.7 could be presented as

$$\nabla(c_1^2\nabla^2\phi - \rho\ddot{\phi}) + \nabla \times (c_2^2\nabla^2\psi - \rho\ddot{\psi}) + \rho\boldsymbol{b} = 0. \tag{3.10}$$

Neglecting the body forces, the above equation is true if the inside bracket terms are equal to zero, which results in wave equations associated with scalar and vector potentials respectively,

$$c_1^2\nabla^2\phi = \ddot{\phi}, \tag{3.11}$$

$$c_2^2\nabla^2\psi = \ddot{\psi}. \tag{3.12}$$

Applying divergence and curl respectively on equation 3.10, gives the general wave equations, where used dilatation part is $\theta = \nabla.\boldsymbol{u} = \nabla^2\phi$ and rotational part is $\omega = -\frac{1}{2}\nabla \times \boldsymbol{u} = -\nabla^2\psi$.

$$c_1^2\nabla^2\theta = \ddot{\theta}, \tag{3.13}$$

$$c_2^2\nabla^2\omega = \ddot{\omega}. \tag{3.14}$$

For time harmonic elasticity, the displacement could be transformed into its real and complex parts: $\boldsymbol{u} = \hat{\boldsymbol{u}}\, e^{i\omega t}$, where $\hat{\boldsymbol{u}}$ is the amplitude of the displacement and ω is the circular frequency.

$$(c_1^2 - c_2^2)\nabla(\nabla.\hat{\boldsymbol{u}}) + c_2^2\nabla^2\hat{\boldsymbol{u}} = -\omega^2\hat{\boldsymbol{u}}. \tag{3.15}$$

$\hat{\boldsymbol{u}} = \boldsymbol{u}$, is taken for generalization.

3.1.2 Integral Representation

The general field equation represented in terms of elasticity tensor from generalized Hooke's law, forms the basic step for obtaining the integral equation.

$$C_{ijkl}u_{k,lj} + \rho b_i \;\; = \;\; \rho\ddot{u}_i. \tag{3.16}$$

With time harmonic motion assumption,

$$C_{ijkl}u_{k,lj} + \rho\omega^2 u_i + \rho b_i \quad = \quad 0. \tag{3.17}$$

The equation 3.17 is in strong form and converted into its weak form by weighted residuals method. Although a step further on weak form, i.e. applying Green's second identity makes the possibility of obtaining the inverse statement helpful to get the representation formula in boundary integral equation. Weighting the equation 3.17 with a test function as fundamental solution u_i^*, we obtain

$$\int_\Omega \left(C_{ijkl}u_{k,lj} + \rho\omega^2 u_i + \rho b_i\right) u_i^* d\Omega = 0. \tag{3.18}$$

Equation 3.18 has the approximation of u and not the exact value of u. Applying Green's first identity to the term $u_{k,lj}$, we obtain

$$\int_\Omega C_{ijkl}u_{k,lj}u_i^* d\Omega = \int_\Omega \left(C_{ijkl}u_{k,l}u_i^*\right)_{,j} d\Omega - \int_\Omega C_{ijkl}u_{k,l}u_{i,j}^* d\Omega. \tag{3.19}$$

Applying divergence theorem to transfer the domain integral to boundary integral,

$$\int_\Omega C_{ijkl}u_{k,lj}u_i^* d\Omega = \int_\Gamma C_{ijkl}u_{k,l}u_i^* n_j d\Gamma - \int_\Omega C_{ijkl}u_{k,l}u_{i,j}^* d\Omega. \tag{3.20}$$

The Green's second identity obtained by once again doing the integration by parts and applying divergence theorem,

$$\begin{aligned}
\int_\Omega C_{ijkl}u_{k,lj}u_i^* d\Omega &= \int_\Gamma C_{ijkl}u_{k,l}u_i^* n_j d\Gamma - \int_\Gamma C_{ijkl}u_k u_{i,j}^* n_l d\Gamma + \int_\Omega C_{ijkl}u_k u_{i,jl}^* d\Omega \\
\int_\Omega C_{ijkl}u_{k,lj}u_i^* d\Omega &= \int_\Gamma C_{ijkl}u_{k,l}n_j u_i^* d\Gamma - \int_\Gamma C_{ijkl}u_{i,j}^* n_l u_k d\Gamma + \int_\Omega C_{ijkl}u_k u_{i,jl}^* d\Omega
\end{aligned} \tag{3.21}$$

Using constitutive equation from Hooke's law $\sigma_{ij} = C_{ijkl}u_{k,l}$ (including the linear relation between strain and displacement), we can rewrite the above equation as

$$\int_\Omega C_{ijkl}u_{k,lj}u_i^* d\Omega - \int_\Omega C_{ijkl}u_k u_{i,jl}^* d\Omega = \int_\Gamma \sigma_{ij}n_j u_i^* d\Gamma - \int_\Gamma \sigma_{kl}^* n_l u_k d\Gamma. \tag{3.22}$$

The above relation could also be obtained from the reciprocal work principle with consideration of 2 domains (Ω and reciprocal domain Ω^*), such that the work done remains same when carried by application of stress state with reciprocal strain and vice versa. The result of same is depicted below

$$\int_\Gamma \sigma_{ij}u_i^* n_j d\Gamma - \int_\Omega \sigma_{ij,j}u_i^* d\Gamma = \int_\Gamma \sigma_{ij}^* u_i n_j d\Gamma - \int_\Omega \sigma_{ij,j}^* u_i d\Omega. \tag{3.23}$$

The method of weighted residual is more generally applicable for any linear differential operator with constant coefficients, on the contrary reciprocal theorem

shows predominance due to its advantage of taking the reciprocal domain Ω^* to infinity. In equation (reciprocal), it could be observed that the differential operator $\left(\frac{\partial^2}{\partial x_l \partial x_j} = \frac{\partial^2}{\partial x_j \partial x_l}\right)$ is self adjoint and taking the symmetrical elastic tensor ($C_{ijkl} = C_{klij}$) into account, the equation becomes

$$\int_\Omega C_{ijkl} u_{k,lj} u_i^* d\Omega - \int_\Omega C_{ijkl} u_{k,lj}^* u_i d\Omega = \int_\Gamma \sigma_{ij} n_j u_i^* d\Gamma - \int_\Gamma \sigma_{ij}^* n_j u_j d\Gamma. \quad (3.24)$$

Using Cauchy law $t_i = \sigma_{ij} n_j$, we obtain

$$\int_\Omega C_{ijkl} u_{k,lj} u_i^* d\Omega - \int_\Omega C_{ijkl} u_{k,lj}^* u_i d\Omega = \int_\Gamma \left(t_i u_i^* - t_i^* u_j\right) d\Gamma \quad (3.25)$$

Adding and subtracting ($\rho\omega^2 u_i u_i^*$) would yield a Helmholtz differential operator on both u and u^*,

$$\int_\Omega C_{ijkl} u_{k,lj} u_i^* d\Omega + \int_\Omega \rho\omega^2 u_i u_i^* d\Omega - \int_\Omega C_{ijkl} u_{k,lj}^* u_i d\Omega - \int_\Omega \rho\omega^2 u_i^* u_i d\Omega = \int_\Gamma \left(t_i u_i^* - t_i^* u_j\right) d\Gamma \quad (3.26)$$

$$\int_\Omega \left(C_{ijkl} u_{k,lj} + \rho\omega^2 u_i\right) u_i^* d\Omega - \int_\Omega \left(C_{ijkl} u_{k,lj}^* + \rho\omega^2 u_i^*\right) u_i d\Omega = \int_\Gamma \left(t_i u_i^* - t_i^* u_j\right) d\Gamma \quad (3.27)$$

Considering the body force term associated with the reciprocal domain (Ω^*) namely b_i^* for the state variables ($\sigma_{ij}^*, u_{i,j}^*$), from equation 3.18, the previous equation could be rewritten in terms of body forces as

$$\int_\Omega \rho \left(b_i^* u_i - b_i u_i^*\right) d\Omega = \int_\Gamma \left(t_i u_i^* - t_i^* u_i\right) d\Gamma. \quad (3.28)$$

For the case of point load of the reciprocal field, the body force is represented as $\rho b_i = \delta(x, \xi) n_i$, where δ represents the Dirac distribution and n_i indicating the direction of applied force. It is important to notice that force when applied in one direction could also produce deformations in other directions (x, y, z) too. Using the sifting property of the Dirac distribution,

$$\int_\Omega \rho b_i^*(x, \xi) u_i(x) d\Omega = \int_\Omega \delta(x, \xi) n_i u_i(x) d\Omega = u_i(\xi) n_i \quad (3.29)$$

For the applied forces in 3 directions, above relation yields only the product of i^{th} component, although there are other components of displacement too present. To have determination of all, it is ensured to have 3 fundamental solution u_i^* in each direction which is represented as u_{mi} meaning that the displacement is measured at a defined point in direction of i when applied load in direction of m. This yields

$$u_i^*(x) = u_{mi}^*(x) n_i. \quad (3.30)$$

Here, m represents the direction of the excitation and i represents the direction in which value being measured. The fundamental equation is hence calculated for displacement tensor u^*_{mi}, such that factor of δ_{ij} is multiplied with Dirac delta distribution, as presented in next topic relating to derivation of fundamental solution. Hence the equation 3.28 could be formed as

$$\begin{aligned} u_{mi}(\xi)n_m n_i - \int_\Omega \rho b_i(x) u^*_{mi}(x,\xi) n_m d\Omega = \int_\Gamma u^*_{mi}(x,\xi) n_m t_i(x) d\Gamma \\ - \int_\Gamma t^*_{mi}(x,\xi) n_m u_i(x) d\Gamma \\ u_m(\xi) - \int_\Omega \rho b_i u^*_{mi} d\Omega = \int_\Gamma u^*_{mi}(x,\xi) t_i(x) d\Gamma - \int_\Gamma t^*_{mi}(x,\xi) u_j(x) d\Gamma \end{aligned} \tag{3.31}$$

For no body forces, the above equation is reduced to body-force free Somigliana identity, also the refereed to representation formula in boundary element method.

$$u_m(\xi) = \int_\Gamma u^*_{mi}(x,\xi) t_i(x) d\Gamma - \int_\Gamma t^*_{mi}(x,\xi) u_i(x) d\Gamma \tag{3.32}$$

3.1.3 Fundamental Solution

The Fundamental solution relates to the solution of differential form $L\boldsymbol{u} = \delta(x,\xi)$ in full space where x and ξ represents the filed vector and load vector respectively. The general field equation for 3D elastodynamics (equation 3.15), could be modified with the substituting the body forces on the reciprocal field to represent the body force term as, $\rho \boldsymbol{b}^*_j = \delta(x,\xi)\delta_{ij}$, where load is applied along direction "i" at a point"j". Hence the equation 3.15 could be reformulated in index notation as

$$(c_1^2 - c_2^2)\boldsymbol{u}^*_{ik,kj} + c_2^2\ \boldsymbol{u}^*_{ij,kk} + \omega^2 \boldsymbol{u}_{ij} = -\frac{1}{\rho}\delta(x,\xi)\delta_{ij} \tag{3.33}$$

Taking c_2^2 common and using $c_2^2 = \dfrac{\mu}{\rho}$, we obtain

$$\left(\frac{c_1^2}{c_2^2} - 1\right)\boldsymbol{u}^*_{ik,kj} + \boldsymbol{u}^*_{ij,kk} + \frac{\omega^2}{c_2^2}\boldsymbol{u}^*_{ij} = -\frac{1}{\mu}\delta(x,\xi)\delta_{ij} \tag{3.34}$$

The aim is to convert the equation above in a form whose fundamental solution is known. One such notion could be to introduce a tensor potential G_{ij} to represent $\boldsymbol{u}^*_{ik}$ as,

$$\boldsymbol{u}^*_{ik} = G_{ij,mm} + \frac{\omega^2}{c_1^2}G_{ij} - \left(1 - \frac{c_2^2}{c_1^2}\right)G_{im,mj} \tag{3.35}$$

Hence, the derivatives of $\boldsymbol{u}_{ik}$ could be simplified with $G_{ik,mmkj} = G_{im,kmkj}$ to the expressions

$$\begin{aligned} \boldsymbol{u}^*_{ik,kj} &= \frac{\omega^2}{c_1^2} G_{ik,kj} + \frac{c_2^2}{c_1^2} G_{im,mkkj}, \\ \boldsymbol{u}^*_{ij,kk} &= G_{ij,mmkk} + \frac{\omega^2}{c_1^2} G_{ij,kk} - \left(1 - \frac{c_2^2}{c_1^2}\right) G_{im,mjkk}. \end{aligned} \tag{3.36}$$

Hence equation 3.34 becomes

$$\left(\frac{c_1^2}{c_2^2} - 1\right)\left[\frac{\omega^2}{c_1^2} G_{ik,kj} + \frac{c_2^2}{c_1^2} G_{im,mkkj}\right] + \left[G_{ij,mmkk} + \frac{\omega^2}{c_1^2} G_{ij,kk} - (1 - \frac{c_2^2}{c_1^2}) G_{im,mjkk}\right] + \frac{\omega^2}{c_2^2}\left[G_{ij,mm} + \frac{\omega^2}{c_1^2} G_{ij} - (1 - \frac{c_2^2}{c_1^2}) G_{im,mj}\right] = -\frac{1}{\mu}\delta(x,\xi)\delta_{ij} \tag{3.37}$$

Simplifying the above equation,

$$G_{ij,mmkk} + \frac{\omega^2}{c_1^2} G_{ij,kk} + \frac{\omega^2}{c_2^2} G_{ij,mm} + \frac{\omega^2}{c_1^2}\frac{\omega^2}{c_1^2} G_{ij} = -\frac{1}{\mu}\delta(x,\xi)\delta_{ij} \tag{3.38}$$

Introducing the definition of wave number as the ratio of circular frequency to the wave speed, $k_1 = \left(\frac{\omega}{c_1}\right)$ and $k_2 = \left(\frac{\omega}{c_2}\right)$, the equation could be written as

$$G_{ij,mmkk} + k_1^2 G_{ij,kk} + k_2^2 G_{ij,mm} + k_1^2 k_2^2 G_{ij} = -\frac{1}{\mu}\delta(x,\xi)\delta_{ij} \tag{3.39}$$

with scalar potential G, such that $G_{ij} = G\delta_{ij}$, the above equation could be represented as

$$\left(\nabla^2 + k_1^2\right)\left(\nabla^2 + k_2^2\right)(G) = -\frac{1}{\mu}\delta(x,\xi) \tag{3.40}$$

Taking $\left(\nabla^2 + k_2^2\right)(G) = F$, would result in a form of Helmholtz equation.

$$\left(\nabla^2 + k_1^2\right) F = -\frac{1}{\mu}\delta(x,\xi) \tag{3.41}$$

Now, we can derive the fundamental solution of Helmholtz differential operator on F, and use it again for the inhomogeneous Helmholtz equation form in G, to get the complete fundamental solution. Transforming equation 3.41 into polar coordinates with assumption of radial symmetry;

$$\frac{1}{r^2}\frac{\partial}{\partial r}\left(r^2 \frac{\partial F}{\partial r}\right) + k^2 F = -\frac{\delta(r)}{4\pi\mu r^2} \tag{3.42}$$

The above equation could be represented as a inhomogeneous Helmholtz equation of (rF)

$$\frac{\partial}{\partial r}\left(\frac{\partial (rF)}{\partial r}\right) + k^2 (rF) = -\frac{\delta(r)}{4\pi\mu r} \tag{3.43}$$

Taking F as dependent only on r,

$$\frac{d^2(rF)}{dr^2} + k^2(rF) = -\frac{\delta(r)}{4\pi\mu r} \tag{3.44}$$

The solution of an differential equation of form $\frac{d^2(y)}{dr^2} + k^2(y) = 0$ is given as, $y = C_1 e^{-ikr} + C_2 e^{ikr}$, here y is replaced by rF, and hence the solution could be presented as

$$F = \frac{C_1 e^{-ikr}}{r} + \frac{C_2 e^{ikr}}{r} \tag{3.45}$$

From Sommerfield radiation condition, it could be concluded that, for large distance r, there are no reflections and hence the part in the Helmholtz solution accounting for reflected waves could be taken to zero. Hence $C_2 = 0$. Also for $r \to 0$, expansion of exponential series with comparison of Laplace fundamental solution yields that $C_1 = \frac{1}{4\pi\mu}$;

$$F = \frac{e^{-ikr}}{4\pi\mu r} \tag{3.46}$$

Now,F could be substituted to get the fundamental solution for inhomogeneous Helmholtz equation in G as.

$$(\nabla^2 + k^2)G = F = \frac{e^{-ikr}}{4\pi\mu r}$$
$$\frac{d^2G}{dr^2} + \frac{2}{r}\frac{dG}{dr} + k_2^2 G = \frac{e^{-ikr}}{4\pi\mu r}$$

The solution of homogeneous part is the general solution of Helmholtz equation

$$G_h = \frac{D_1 e^{-ikr}}{r} + \frac{D_2 e^{ikr}}{r} \tag{3.47}$$

here considering the variation of constants as k_1 could be replaced with k_2 in previous relations, it results in coefficients D_1 and D_2 with $(a = 1, b = 2)$ and $(a = 2, b = 1)$.

$$D_1(r) = \frac{1}{8\pi\mu k_b(k_b - k_a)} e^{-ir(k_b - k_a)} \qquad D_2(r) = \frac{1}{8\pi\mu k_b(k_b + k_a)} e^{-ir(k_b + k_a)} \tag{3.48}$$

From here, the particular part of solution is obtained as

$$G_h(r) = \frac{1}{4\pi\mu(k_b^2 - k_a^2)} e^{-irk_a} \tag{3.49}$$

Hence the tensor G could be represented as

$$G_{ij}(r) = \frac{1}{4\pi\mu(k_2^2 - k_1^2)} \frac{e^{-irk_1} - e^{-irk_2}}{r} \delta_{ij} \tag{3.50}$$

The above result could be substituted in equation 3.35 to obtain the fundamental solution of displacement as

$$\boldsymbol{u}^*_{ij} = \frac{1}{4\pi\mu}(\psi\delta_{ij} - \chi r_{,i} r_{,j}) \tag{3.51}$$

where

$$\begin{aligned}
\psi &= \left[1 + \frac{1}{(ik_2 r)^2} + \frac{1}{(ik_2 r)}\right]\frac{e^{-ik_2 r}}{r} - \frac{k_1^2}{k_2^2}\left[1 + \frac{1}{(ik_1 r)^2} + \frac{1}{(ik_1 r)}\right]\frac{e^{-ik_1 r}}{r} \\
\chi &= \left[1 + \frac{3}{(ik_2 r)^2} + \frac{3}{(ik_2 r)}\right]\frac{e^{-ik_2 r}}{r} - \frac{k_1^2}{k_2^2}\left[1 + \frac{3}{(ik_1 r)^2} + \frac{3}{(ik_1 r)}\right]\frac{e^{-ik_1 r}}{r}
\end{aligned} \tag{3.52}$$

The traction field could be obtained by taking the directional derivative of the displacement field.

$$\begin{aligned}
\boldsymbol{t}^*_{ij} \;=\; & \frac{1}{4\pi}[(\frac{d\psi}{dr} - \frac{1}{r}\chi)(\delta_{ij}\frac{\partial r}{\partial n} + r_{,j} n_{,i}) - \frac{2}{r}\chi(n_j r_{,i} - 2r_{,i} r_{,j}\frac{\partial r}{\partial n}) - 2\frac{d\chi}{dr} r_{,i} r_{,j}\frac{\partial r}{\partial n} + \\
& (\frac{{c_1}^2}{{c_2}^2} - 2)(\frac{d\psi}{dr} - \frac{d\chi}{dr} - \frac{2\chi}{r}) r_{,i} n_{,j}]
\end{aligned} \tag{3.53}$$

Both displacement and tractions have been functions of ψ and χ, which contains exponential terms. A series exponential expansion would reduce the two as

$$\begin{aligned}
\psi &= \frac{1}{2r}\left(1 + \frac{{c_2}^2}{{c_1}^2}\right) + ik_2 \sum_{n=0}^{\infty} \frac{1}{(n+1)(n+3)}\left[n + 2 + \left(\frac{{c_2}^2}{{c_1}^2}\right)^{n+3}\right]\frac{(ik_2 r)^n}{n!} \\
\chi &= -\frac{1}{2r}\left(1 - \frac{{c_2}^2}{{c_1}^2}\right) + ik_2 \sum_{n=0}^{\infty} \frac{n}{(n+1)(n+3)}\left[1 - \left(\frac{{c_2}^2}{{c_1}^2}\right)^{n+3}\right]\frac{(ik_2 r)^n}{n!}
\end{aligned} \tag{3.54}$$

Substitution of obtained ψ and χ into displacement fields show that it converges with the elastostatics fundamental solution of displacement fields. These functions so can be split as

$$\begin{aligned}
\psi &= \frac{1}{2r}(1 + \frac{{c_2}^2}{{c_1}^2}) + O(k_2) \\
\chi &= -\frac{1}{2r}(1 - \frac{{c_2}^2}{{c_1}^2}) + O(k_2)
\end{aligned} \tag{3.55}$$

To analyze the low frequency behavior of the tractions one can rewrite equation 3.53 as

$$\boldsymbol{t}^*_{ij} = \frac{1}{4\pi}[\boldsymbol{A}(\frac{\partial r}{\partial n}\delta_{ij} + r_{,j} n_{,i}) + r_{,i} r_{,j}\frac{\partial r}{\partial n}\boldsymbol{B} + r_{,i} n_{,j}\boldsymbol{C}] \tag{3.56}$$

where,

$$\begin{aligned}
\boldsymbol{A} &= \frac{d\psi}{dr} - \frac{\chi}{r} \\
\boldsymbol{B} &= \frac{4\chi}{r} - 2\frac{d\chi}{dr} \\
\boldsymbol{C} &= (\frac{{c_1}^2}{{c_2}^2} - 2)(\frac{d\psi}{dr} - \frac{d\chi}{dr} - 2\frac{\chi}{r}) - 2\frac{\chi}{r}
\end{aligned} \tag{3.57}$$

Substitution of exponentials by their series expansions gives for the above terms

$$\begin{aligned}
\boldsymbol{A} &= -\frac{1}{r^2}\frac{{c_2}^2}{{c_1}^2} + {k_2}^2 \sum_{n=0}^{\infty} \frac{n+2[1+(c_2/c_1)^{n+4}]}{(n+2)(n+4)} \frac{(k_2 r)^n}{n!} \\
\boldsymbol{B} &= -\frac{3}{r^2}(1 - \frac{{c_2}^2}{{c_1}^2}) - {k_2}^2 \sum_{n=0}^{\infty} \frac{2(n-1)}{(n+2)(n+4)} [1-(c_2/c_1)^{n+4}] \frac{(k_2 r)^n}{n!} \\
\boldsymbol{C} &= \frac{1}{r^2}\frac{{c_2}^2}{{c_1}^2} + {k_2}^2 \sum_{n=0}^{\infty} \frac{-2+(n+4)(c_2/c_1)^{n+2} - 2(n+3)(c_2/c_1)^{n+4}}{(n+2)(n+4)} \frac{(k_2 r)^n}{n!}
\end{aligned} \tag{3.58}$$

Which could also be presented with splitting the singular and nonsingular terms as

$$\begin{aligned}
\boldsymbol{A} &= -\frac{1}{r^2}\frac{{c_2}^2}{{c_1}^2} + O({k_2}^2) \\
\boldsymbol{B} &= -\frac{3}{r^2}(1 - \frac{{c_2}^2}{{c_1}^2}) + O({k_2}^2) \\
\boldsymbol{C} &= \frac{1}{r^2}\frac{{c_2}^2}{{c_1}^2} + O({k_2}^2)
\end{aligned} \tag{3.59}$$

Similarly, for $k_2 \to 0$ the results coincide with the elastostatics fundamental solution for traction fields.

3.1.4 Boundary Integral equation

The displacement at any point ξ inside the domain could be calculated once the displacements and tractions on the boundary are known, as shown in representation formula equation 3.32. The Dirac distribution property holds valid only inside domain, and not onto boundary.

$$\int g(s)\delta(s,\xi) = \begin{cases} g(\xi) & \text{if } \xi \in \Omega \\ 0 & \text{if } \xi \notin \Omega \ , \ \xi \notin \Gamma \\ \text{undefined} & \text{if } \xi \in \Gamma \end{cases} \tag{3.60}$$

But the representation formula is valid for complete domain including the boundary. Hence, ξ could be taken to boundary to calculate the unknown terms associated with displacement and traction fields with special considerations. When

$\xi \in \Gamma$ i.e. $(r \to 0)$, the fundamental solution presented above shows singular behavior. One method to transfer load point onto boundary without much loss of Dirac property, is to extend the boundary with symmetric shape body element. For smooth boundary a hemisphere in three dimensional and semicircle in two dimensional case could be chosen, such that the load point on the old boundary is equidistant from the boundary of the extended part as shown in figure 3.1. The

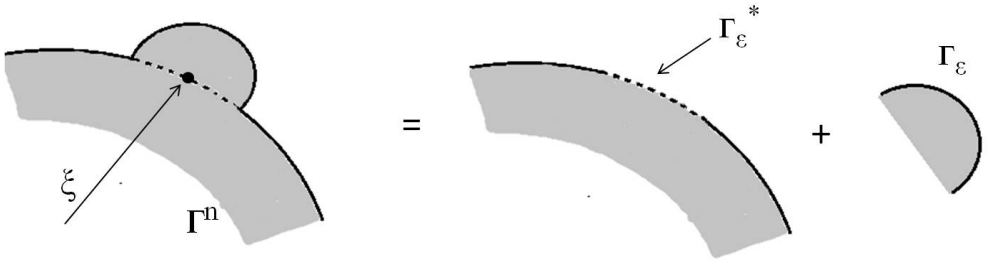

Figure 3.1: Extended boundary in 2D with semicircle around the load point ξ

new domain boundary Γ^n could be expressed as

$$\Gamma^n = \Gamma - \Gamma_\varepsilon^* + \Gamma_\varepsilon \tag{3.61}$$

where Γ represents the original boundary of domain, with extended domain having the boundary as Γ_ε and Γ_ε^* being the interface. The above relation holds true for the condition $\Gamma = \lim_{\varepsilon \to 0} \Gamma^n$, where ε represents the radius of the extended boundary with center as the load point.

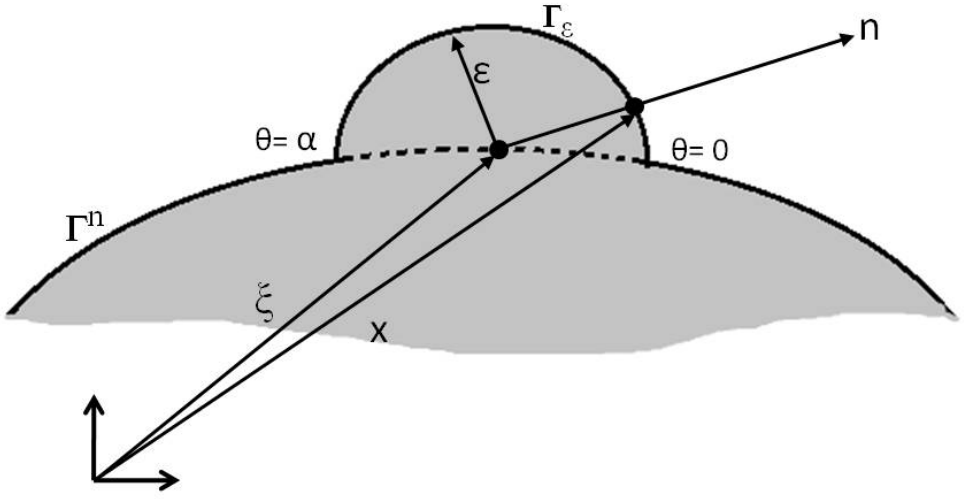

Figure 3.2: Geometry of extended domain ξ

The figure 3.2 represents the geometry of the extended domain, and it could be observed the angle made by normal vector n at the field point X is π, for smooth boundaries with constant element.

The representation formula could now be expressed on the new domain as

$$\begin{aligned} u_m(\xi) &= \lim_{\varepsilon\to 0}\int_{\Gamma-\Gamma^*_\varepsilon} u^*_{mi}(x,\xi)t_i(x)d(\Gamma-\Gamma^*_\varepsilon) - \int_{\Gamma-\Gamma^*_\varepsilon} t^*_{mi}(x,\xi)u_i(x)d(\Gamma-\Gamma^*_\varepsilon) + \\ &\quad \lim_{\varepsilon\to 0}\int_{\Gamma_\varepsilon} u^*_{mi}(x,\xi)t_i(x)d\Gamma_\varepsilon - \lim_{\varepsilon\to 0}\int_{\Gamma_\varepsilon} t^*_{mi}(x,\xi)u_i(x)d\Gamma_\varepsilon \end{aligned} \tag{3.62}$$

Observing the fundamental solution of displacement and traction field, it is evident that the displacement field contains singularity of $(1/r)$ and traction field containing the singularity of $(1/r^2)$ which are weak and strong singularities respectively. More about the treatment of same are dealt in topics associated with numerical integration. Hence the fundamental solution could be presented in a form

$$\begin{aligned} u^*_{mi} &= \frac{1}{r}u_{mi}{}' \\ t^*_{mi} &= \frac{1}{r^2}t'_{mi} \end{aligned} \tag{3.63}$$

where u'_{mi} and t'_{mi} are the terms containing no singularity and $r = x - \xi = \varepsilon$. The above expressions could be also expressed in polar coordinated to have ease in determination of elemental area in polar coordinates as $\Gamma_\varepsilon = r^2\sin\theta\ d\theta\ d\phi$. Where,

$$\begin{aligned} &r = \sqrt{x^2+y^2+z^2} \\ &x = r\ \cos\theta\ \sin\phi\ \ ;\ \ y = r\ \sin\theta\ \sin\phi\ \ ;\ \ z = r\ \cos\phi. \end{aligned} \tag{3.64}$$

From above, the nonsingular terms in fundamental solution also can be expressed in polar coordinates with dependence only on ϕ and θ, with normal vector being in direction of r such that $n_i = r_{,i} = \dfrac{\partial r}{\partial r_i} = [\cos\theta\ \sin\phi\ \ ,\ \sin\theta\ \sin\phi\ \ ,\ \cos\phi]^T$ The terms associated with the extended boundary Γ_ε could be simplified with above considerations

$$\begin{aligned} \lim_{\varepsilon\to 0}\int_{\Gamma_\varepsilon} u^*_{mi}(x,\xi)t_i(x)d\Gamma_\varepsilon &= \lim_{r\to 0}\int_\phi\int_\theta \left(\frac{u'_{mi}(\theta,\phi)}{r}r^2\sin\theta\ d\theta\ d\phi\right)t_i \\ &= \lim_{r\to 0}\int_\phi\int_\theta \left(u'_{mi}(\theta,\phi)r\sin\theta\ d\theta\ d\phi\right)t_i \\ &= 0 \\ \lim_{\varepsilon\to 0}\int_{\Gamma_\varepsilon} t^*_{mi}(x,\xi)u_i(x)d\Gamma_\varepsilon &= \lim_{r\to 0}\int_\phi\int_\theta \left(\frac{t'_{mi}(\theta,\phi)}{r^2}r^2\sin\theta\ d\theta\ d\phi\right)u_i \\ &= \lim_{r\to 0}\int_\phi\int_\theta \left(t'_{mi}(\theta,\phi)\sin\theta\ d\theta\ d\phi\right)u_i \\ &= c_{mi}u_i \end{aligned} \tag{3.65}$$

Here, c_{mi} is referred as constant free term. For a smooth boundary with $0 \leq \theta < \pi/2$ and $0 \leq \phi < 2\pi$, $c_{mi} = -\frac{1}{2}\delta_{mi}$. Replacing obtained expression in equation 3.62, the representation formula is expressed in simplified boundary integral equation

$$c_{mi}(\xi)u_i(\xi) + \cancel{\int}_{\Gamma} t^*_{mi}(x,\xi)u_i(x)d\Gamma = \int_{\Gamma} u^*_{mi}(x,\xi)t_i(x)d\Gamma \tag{3.66}$$

where, $\cancel{\int}_{\Gamma} t^*_{mi}u_i d\Gamma$ is the Cauchy principle value integral and

$$c_{mi} = \delta_{mi} + \lim_{r\to 0}\int_{\Gamma_\varepsilon} t^{'}_{mi}d\Gamma \tag{3.67}$$

The equation 3.66 is the basic boundary integral elastodynamics equation in 3D and forms the basis for determination of field variables simultaneously. The Numerical methods are used to solve the equation using the conventional shape functions with known boundary conditions. The numerical treatment follows in next chapter.

4 Implementation

4.1 Numerical Implementation of BIE

The available boundary integral equation is discretized into finite elements to approximate the solution for actual boundary value problem with given boundary conditions. The collocation point weighted residual method is used as the numerical approximation, where as Galerkin method could also be used which gives the advantage of symmetric matrix system to solve but require more computational efforts. The finite elements used to discretize the boundary are called boundary elements as the unknown variables are on the boundary and hence to solve a 3D boundary value problem we would require only 2D surface elements on the boundary of the 3D domain. This reduces the order of system of equations to be solved for.

4.1.1 Boundary Elements

As we require only 2D surface elements for 3D domain's boundary, our concentration would be more on the same. The mostly used 2D surface elements are quadrilateral and triangle. The discretized boundary into E number of finite elements could be represented as

$$\Gamma = \sum_{e=1}^{E} \Gamma^e. \tag{4.1}$$

As the shape functions are described in local coordinates, the variables associated with the Cartesian coordinates are transformed to the local coordinates as

$$x^e(\eta, \xi) = \sum_{m=1}^{n} \phi_m x_m^e \tag{4.2}$$

where, e refers to the specific element with n number of nodes. With the isoparametric concept, the same shape functions could be used to approximate the boundary field variables.

$$\begin{aligned} u^e(\eta, \xi) &= \sum_{m=1}^{n} \phi_m u_m^e \\ t^e(\eta, \xi) &= \sum_{m=1}^{n} \phi_m t_m^e \end{aligned} \tag{4.3}$$

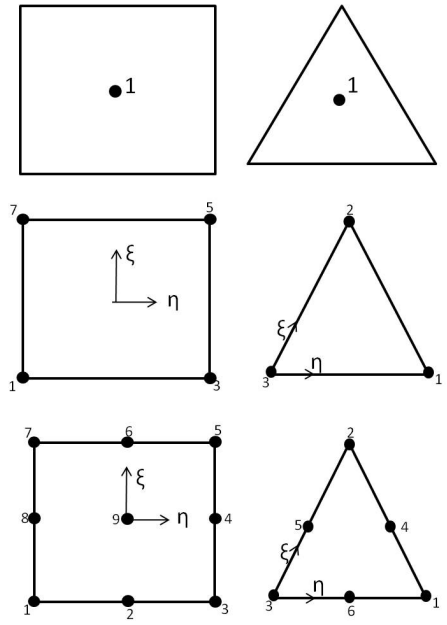

Figure 4.1: a)Constant 2D element b) Linear 2D element c) Bilinear quadratic 2D element

Table 4.1: Element table

Order	Quadrilateral	Triangular
Constant	$\phi_1 = 1$	$\phi_1 = 1$
Linear	$\phi_1 = (1/4)(1-\eta)(1-\xi)$ $\phi_2 = (1/4)(1+\eta)(1-\xi)$ $\phi_3 = (1/4)(1-\eta)(1+\xi)$ $\phi_4 = (1/4)(1+\eta)(1+\xi)$	$\phi_1 = \eta$ $\phi_2 = \xi$ $\phi_3 = 1-\eta-\xi$
Bi-Quadratic	$\phi_1 = \eta(2\eta-1)$ $\phi_2 = \xi(2\eta-1)$ $\phi_3 = (1-\eta-\xi)(2(1-\eta-\xi)-1)$ $\phi_4 = (1/2)\eta(1+\eta)(1-\xi^2)$ $\phi_5 = (1/4)\eta(\eta+1)\xi(\xi+1)$ $\phi_6 = (1/2)(1-\eta^2)\xi(\xi+1)$ $\phi_7 = (1/4)\eta(\eta-1)\xi(\xi+1)$ $\phi_8 = (1/2)\eta(\eta-1)(1-\xi^2)$ $\phi_9 = (1-\eta^2)(1-\xi^2)$	$\phi_1 = (1/4)\eta(\eta-1)\xi(\xi-1)$ $\phi_2 = (1/2)(1-\eta^2)\xi(\xi-1)$ $\phi_3 = (1/4)\eta(1+\eta)\xi(\xi-1)$ $\phi_4 = 4\eta\xi$ $\phi_5 = 4\xi(1-\eta-\xi)$ $\phi_6 = 4(1-\xi-\eta)\eta$

More about the transformation for evaluation of integrals are discussed in next section. Now introducing the discretized boundary to approximate the integrals, the representation formula is expressed in matrix form as

$$\underline{\boldsymbol{c}}\boldsymbol{u} + \fint_{\Gamma} \underline{\boldsymbol{t}}^{*}\boldsymbol{u}\, d\Gamma = \int_{\Gamma} \underline{\boldsymbol{u}}^{*}\boldsymbol{t}\, d\Gamma \tag{4.4}$$

where,

$$\underline{\boldsymbol{u}}^* = \begin{bmatrix} \boldsymbol{u}^*_{11} & \boldsymbol{u}^*_{12} & \boldsymbol{u}^*_{13} \\ \boldsymbol{u}^*_{21} & \boldsymbol{u}^*_{22} & \boldsymbol{u}^*_{23} \\ \boldsymbol{u}^*_{31} & \boldsymbol{u}^*_{32} & \boldsymbol{u}^*_{33} \end{bmatrix} \qquad \underline{\boldsymbol{t}}^* = \begin{bmatrix} \boldsymbol{t}^*_{11} & \boldsymbol{t}^*_{12} & \boldsymbol{t}^*_{13} \\ \boldsymbol{t}^*_{21} & \boldsymbol{t}^*_{22} & \boldsymbol{t}^*_{23} \\ \boldsymbol{t}^*_{31} & \boldsymbol{t}^*_{32} & \boldsymbol{t}^*_{33} \end{bmatrix} \tag{4.5}$$

$$\boldsymbol{u} = \begin{bmatrix} \boldsymbol{u}_1 \\ \boldsymbol{u}_2 \\ \boldsymbol{u}_3 \end{bmatrix} \qquad \boldsymbol{t} = \begin{bmatrix} \boldsymbol{t}_1 \\ \boldsymbol{t}_2 \\ \boldsymbol{t}_3 \end{bmatrix} \tag{4.6}$$

$\underline{\boldsymbol{c}} = 1/2I$ for the boundary points where the boundary is smooth and $\underline{\boldsymbol{c}} = I$ for internal points, I being the unit 3×3 diagonal matrix. In general,

$$\underline{\boldsymbol{c}} = \begin{bmatrix} c_{11} & c_{12} & c_{13} \\ c_{21} & c_{22} & c_{23} \\ c_{31} & c_{32} & c_{33} \end{bmatrix}$$

$$\boldsymbol{u} = \begin{bmatrix} \boldsymbol{u}_1 \\ \boldsymbol{u}_2 \\ \boldsymbol{u}_3 \end{bmatrix} = \begin{bmatrix} \phi_1 & 0 & 0 & \phi_2 & 0 & 0 & ... & \phi_N & 0 & 0 \\ 0 & \phi_1 & 0 & 0 & \phi_2 & 0 & ... & 0 & \phi_N & 0 \\ 0 & 0 & \phi_1 & 0 & 0 & \phi_2 & ... & 0 & 0 & \phi_N \end{bmatrix} \begin{bmatrix} \boldsymbol{u}^1_1 \\ \boldsymbol{u}^1_2 \\ \boldsymbol{u}^1_3 \\ . \\ . \\ \boldsymbol{u}^N_1 \\ \boldsymbol{u}^N_2 \\ \boldsymbol{u}^N_3 \end{bmatrix} \tag{4.7}$$

$$\boldsymbol{t} = \begin{bmatrix} \boldsymbol{t}_1 \\ \boldsymbol{t}_2 \\ \boldsymbol{t}_3 \end{bmatrix} = \begin{bmatrix} \phi_1 & 0 & 0 & \phi_2 & 0 & 0 & ... & \phi_N & 0 & 0 \\ 0 & \phi_1 & 0 & 0 & \phi_2 & 0 & ... & 0 & \phi_N & 0 \\ 0 & 0 & \phi_1 & 0 & 0 & \phi_2 & ... & 0 & 0 & \phi_N \end{bmatrix} \begin{bmatrix} \boldsymbol{t}^1_1 \\ \boldsymbol{t}^1_2 \\ \boldsymbol{t}^1_3 \\ . \\ . \\ \boldsymbol{t}^N_1 \\ \boldsymbol{t}^N_2 \\ \boldsymbol{t}^N_3 \end{bmatrix} \tag{4.8}$$

Writing the matrix assembly on load point ξ^l,

$$\begin{aligned}\underline{\boldsymbol{c}}(\xi^l)\boldsymbol{u}(\xi^l) + \sum_{e=1}^{E}\sum_{m=1}^{n}\left(\int_{\Gamma^{(e)}} \underline{\boldsymbol{t}}^*(x,\xi^l)\ \phi_m(x)\ d\Gamma\right)\boldsymbol{u}_m^{(e)} \\ = \sum_{e=1}^{E}\sum_{m=1}^{n}\left(\int_{\Gamma^{(e)}} \underline{\boldsymbol{u}}^*(x,\xi^l)\ \phi_m(x)\ d\Gamma\right)\boldsymbol{t}_m^{(e)}\end{aligned} \tag{4.9}$$

Consecutive numbering of global nodes replaces the double summation by a summation over all global nodes N.

$$\underline{\boldsymbol{c}}(\xi^l)\boldsymbol{u}(\xi^l) + \sum_{n=1}^{N}\boldsymbol{H}_{ln}\boldsymbol{u}_n = \sum_{n=1}^{N}\boldsymbol{G}_{ln}\boldsymbol{t}_n \tag{4.10}$$

where,

$$\begin{aligned}\boldsymbol{H}_{ln} &= \int_{\Gamma^{(n,e)}} \underline{\boldsymbol{t}}^*(x,\xi^l)\ \phi_n(x)d\Gamma \quad \text{and} \\ \boldsymbol{G}_{ln} &= \int_{\Gamma^{(n,e)}} \underline{\boldsymbol{u}}^*(x,\xi^l)\ \phi_n(x)d\Gamma\end{aligned} \tag{4.11}$$

For $n = l$, which corresponds to the diagonal entries of $\boldsymbol{H}$ and $\boldsymbol{G}$ matrices, strong and weak singular integrals exist in $\boldsymbol{H}$ and $\boldsymbol{G}$ matrices respectively. For$N$ unknown boundary variables, the equation system could be expressed in as

$$\begin{bmatrix} \hat{\boldsymbol{H}}_{11} & \dots & \boldsymbol{H}_{1i} & \dots & \boldsymbol{H}_{1N} \\ \vdots & \ddots & \vdots & & \vdots \\ \boldsymbol{H}_{i1} & \dots & \hat{\boldsymbol{H}}_{ii} & \dots & \boldsymbol{H}_{iN} \\ \vdots & \ddots & \vdots & & \vdots \\ \boldsymbol{H}_{N1} & \dots & \boldsymbol{H}_{Ni} & \dots & \hat{\boldsymbol{H}}_{NN} \end{bmatrix} \begin{bmatrix} \boldsymbol{u}_1 \\ \vdots \\ \boldsymbol{u}_i \\ \vdots \\ \boldsymbol{u}_N \end{bmatrix} = \begin{bmatrix} \boldsymbol{G}_{11} & \dots & \boldsymbol{G}_{1i} & \dots & \boldsymbol{G}_{1N} \\ \vdots & \ddots & \vdots & & \vdots \\ \boldsymbol{G}_{i1} & \dots & \boldsymbol{G}_{ii} & \dots & \boldsymbol{G}_{iN} \\ \vdots & \ddots & \vdots & & \vdots \\ \boldsymbol{G}_{N1} & \dots & \boldsymbol{G}_{Ni} & \dots & \boldsymbol{G}_{NN} \end{bmatrix} \begin{bmatrix} \boldsymbol{t}_1 \\ \vdots \\ \boldsymbol{t}_i \\ \vdots \\ \boldsymbol{t}_N \end{bmatrix} \tag{4.12}$$

$$\boldsymbol{H}\boldsymbol{u} = \boldsymbol{G}\boldsymbol{t} \tag{4.13}$$

with $\hat{\boldsymbol{H}} = \underline{\boldsymbol{c}}_l + \boldsymbol{H}_{ll}$

4.1.2 Numerical Integration

Boundary element method involves integrals associated with the calculations of $\boldsymbol{H}$ and $\boldsymbol{G}$ matrices whose integrands are the contributions of fundamental solution of primary and secondary variable and shape functions. The integration is carried out depending upon the relative position load point ξ to the boundary element. The numerical integration scheme using Gauss quadrature rule is used for the regular integrals but when the integration point coincides with the load point, there would be cases of weak and strong singularity in fundamental solutions. Below are explained ways for numerical integration of the possible cases featuring in boundary elements.

4.1.2.1 Regular Integrals Gaussian Quadrature

If n points are considered, an $(n+1)^{st}$- degree polynomial can be fit to the n points and integrated. The resulting formulas have the form:

$$\boldsymbol{I} = \int_a^b f(x)dx = \sum_{i=1}^{n} W_i f(x_i) \tag{4.14}$$

where x_i are the locations at which integrand function $f(x)$ is known and W_i are the weighting functions. Here, for n points, it could be observed that $2n$ parameters are available and it makes possible to fit a polynomial of degree $2n-1$. To integrate exactly a polynomial of degree $2n-1$, proper choice of x_i and W_i is required and which forms the Gauss quadrature formula by transforming the integral of function F in limits [-1,1].

$$\boldsymbol{I} = \int_{-1}^{-1} F(s)ds = \sum_{i=1}^{n} W_i F(s_i) \tag{4.15}$$

The multidimensional integrals can be calculated by the tensor product of the one-dimensional quadrature formula. The two dimensional integral is integrated on the reference square $[-1,1] \times [-1,1]$ and similarly the three dimensional on reference cube.

$$\int_{-1}^{1}\int_{-1}^{1} f(\xi,\eta)d\xi d\eta \approx \sum_{i=1}^{n_1}\sum_{j=1}^{n_2} f(\xi_i,\eta_j)W_i W_j \tag{4.16}$$

$$\int_{-1}^{1}\int_{-1}^{1}\int_{-1}^{1} f(\xi,\eta,\zeta)d\xi d\eta d\zeta \approx \sum_{i=1}^{n_1}\sum_{j=1}^{n_2}\sum_{k=1}^{n_3} f(\xi_i,\eta_j,\zeta_k)W_i W_j W_k \tag{4.17}$$

Each boundary element of the original domain has to be transformed to the reference element, which could be obtained by introducing the term of Jacobian defined as the norm of the normal vector pointing outwards at the quadrature points of the element. Figure 4.2 shows the transformation to the local coordinates.

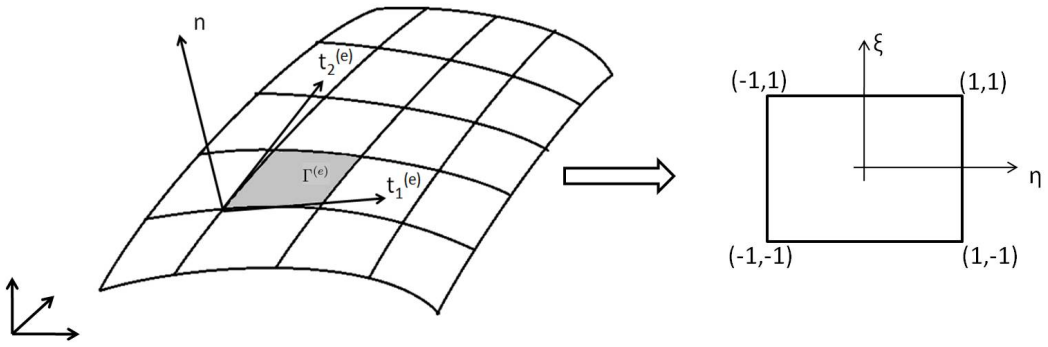

Figure 4.2: Transformation from global system to local system

$$d\Gamma^{(e)} = J^{(e)} ds_1 ds_2 \tag{4.18}$$

where s_1 and s_2 represents the local coordinates of the element. These would be equated to the quadrature points for the integral calculation for the local element. Also, Jacobian could be obtained as follows:

$$J^{(e)} = |t_1^{(e)} \times t_2^{(e)}| \tag{4.19}$$

here $t_1^{(e)} \times t_2^{(e)}$ gives the normal vector at position (s_1, s_2), and the tangential vectors are obtained by:

$$t_1^{(e)} := \frac{\partial \boldsymbol{X}^{(e)}}{\partial s_1} \quad = \quad t_2^{(e)} := \frac{\partial \boldsymbol{X}^{(e)}}{\partial s_2} \tag{4.20}$$

where $\boldsymbol{X}^{(e)}$ denotes the position vector from global coordinates to the local element. The partial derivatives could be obtained from the knowledge of boundary elements discretized with shape functions covered in section of discretization of boundary elements.

For 2D case,

$$\begin{aligned} \int_{\Gamma^{(e)}} f(x_1, x_2, x_3) d\Gamma &= \int_{-1}^{1} \int_{-1}^{1} f(x_1(\xi,\eta), x_2(\xi,\eta), x_3(\xi,\eta)) J(\xi_i, \eta_i) d\xi d\eta \\ &= \sum_{i=1}^{n_1} \sum_{j=1}^{n_2} f(x_1(\xi_i,\eta_i), x_2(\xi_i,\eta_i), x_3(\xi_i,\eta_i)) J(\xi_i, \eta_i) W_i W_j \end{aligned} \tag{4.21}$$

4.1.2.2 Weak and Strong Singularities

The singularity exists when the collocation point or the integration point coincides with the load point. If the integration exists but function is not continuous at load point, it is referred to weak singularity. If both integral and function aren't continuous at the load point, it refers to strong singularity. The $\boldsymbol{H}$ matrix contains the contributions of secondary variables (here tractions) involving strong singularity at the diagonal terms. Weak singularity is observed in the primary variable (here displacement). For constant eleents, the weak singularity exists at diagonals terms of $\boldsymbol{G}$ matrix, for other elements, arbitrarily distributed in combination of load point and integration point. Weak and strong singularity terms present in fundamental solutions are presented below.

$$\begin{array}{rcc} & 2D & 3D \\ WeakSingularity & \ln r & 1/r \\ StrongSingularity & 1/r & 1/r^2 \end{array} \tag{4.22}$$

where, r denotes the distance between the position vector of a node in boundary element and the load point. The weak singularity issues could be resolved by

regularising the transformation for example transformation to polar coordinates, Lachat-Watson transformation. Due to use of Cartesian coordinate system, later is used here. Regularising Transformation refer to the transformation of the the domain such that the contribution from Jacobian would cancel out the effect of weak singularity term , as shown below.

$$\int\int \frac{f(x,y)}{r} dxdy = \int\int f(\xi,\eta)\frac{J}{r} d\xi d\eta \tag{4.23}$$

The integral is regularized with J canceling the term r in denominator and regularizing the integral for $\lim_{r\to 0} J = 0$. The Lachat and Watson method transformation is applied to triangle. The figure 4.3 below shows different possibility of dividing the reference element into triangles pertaining to singular points. The resulted subdivided triangles are transformed to local coordinates of a quadrilateral whose two sides are merged (or two corner points) to single side at the collocation point. This quadrilateral with 2 points having same coordinates, produces the Jacobian magnitude to zero of type r to eliminate the effect of weak singular term $1/r$.

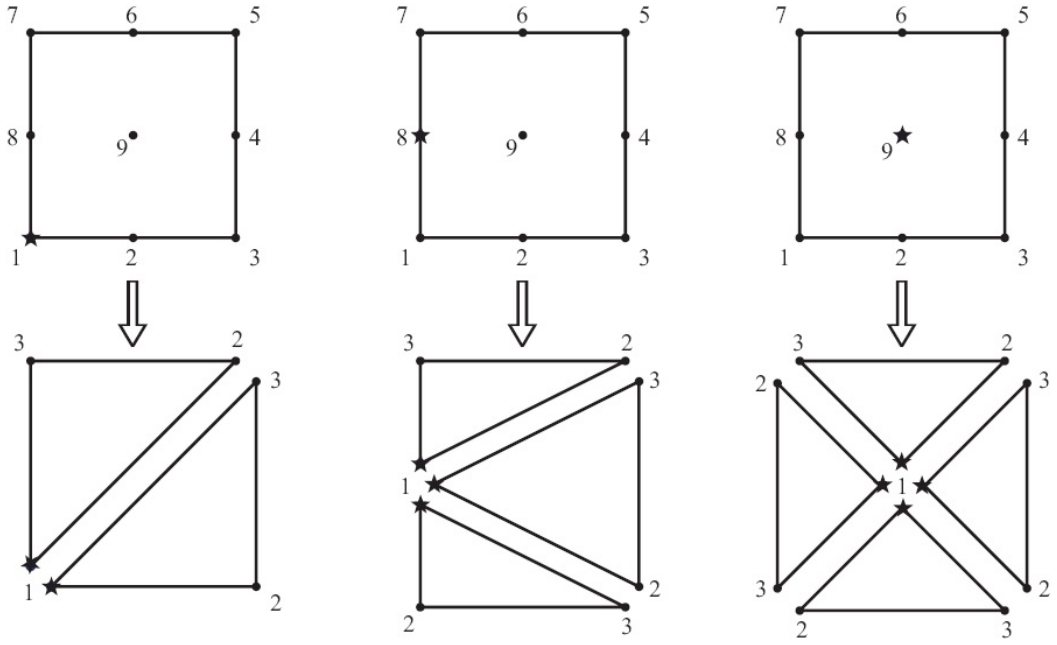

Figure 4.3: Possibilities of division of 2D Quad element into triangular elements

Strong Singularity treatment: Using the Cauchy principle value, the integral was split into constant free term and cauchy integral part.

$$[\hat{\boldsymbol{H}}_s]_{jj} = [\boldsymbol{c}_s]_j + [\boldsymbol{H}_s]_{jj} \tag{4.24}$$

Although there are various methods to calculate Cauchy Principle Value problem numerically, but due to difficulties in the calculation of constant free term in cases of non smooth boundary, here we take use of indirect calculation of diagonal entries of $\boldsymbol{H}$ matrix (Gaul and Schweizer (1998)), which eventually contains

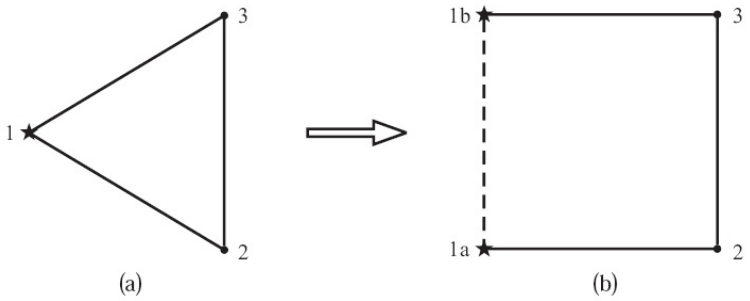

Figure 4.4: Transforming triangular element to quad with Jacobian = 0

the strong singularity. The diagonal entries in statics calculated for by taking constant displacements and zero traction for rigid body motion.

$$\boldsymbol{H}\underline{1} = \boldsymbol{G}\underline{0} \tag{4.25}$$

From above equation the diagonal entries of $\boldsymbol{H}$ matrice could be obtained as the negative sum of the off diagonal terms, as shown below.

$$[\hat{\boldsymbol{H}}_s]_{jj} = -\sum_{n=1;n\neq j} [\boldsymbol{H}_s]_{jn} \tag{4.26}$$

But the above is valid only for elastostatics but not for elastodynamics, as variables are dependent on the time. However, the diagonal terms of elastodynamics case could also be split into constant free term and integral part as

$$[\hat{\boldsymbol{H}}]_{jj} = [\boldsymbol{c}]_j + [\boldsymbol{H}]_{jj} \tag{4.27}$$

The independent free term c here is same as the free term of static case.

$$[\boldsymbol{c}] = [\boldsymbol{c}_s] \tag{4.28}$$

The above statement is quiet evident as reported by [ref Gaul and Fiedler] that as $r \to 0$ is same as $\omega \to 0$. It follows

$$\begin{aligned} \lim_{r\to 0} \boldsymbol{t}^*(x,\xi) &= \lim_{\omega\to 0} \boldsymbol{t}^*(x,\xi) \\ &= \mathbf{t}_s^*(x,\xi) \end{aligned} \tag{4.29}$$

So, that the constant free term for dynamic case could be obtained as

$$\begin{aligned} \boldsymbol{c} &= \boldsymbol{I} + \lim_{\epsilon\to 0} \int_{\Gamma_\epsilon} \boldsymbol{t}_s(x,\xi) d\Gamma_x \\ &= \boldsymbol{c}_s \end{aligned} \tag{4.30}$$

From equation 4.24, equation 4.26 and equaion 4.28

$$[\boldsymbol{c}]_j = [\boldsymbol{c}_s]_j = -\sum_{n=1;n\neq j} [\boldsymbol{H}_s]_{jn} - [\boldsymbol{H}_s]_{jj} \tag{4.31}$$

and hence the result could be replaced in equation 4.27 to obtain the diagonal terms of $\boldsymbol{H}$ matrix for elastodynamic case.

$$[\hat{\boldsymbol{H}}]_{jj} = -\sum_{n=1;n\neq j} [\boldsymbol{H}_s]_{jn} + ([\boldsymbol{H}]_{jj} - [\boldsymbol{H}_s]_{jj}) \tag{4.32}$$

The difference $([\boldsymbol{H}]_{jj} - [\boldsymbol{H}_s]_{jj})$ is the difference of the dynamic and static fundamental traction solution over an element. Individual terms are singular in nature but the difference would cancel the singularity term and leaves with the series expansion term as shown in theory related to fundamental solution for elastodynaimcs.

5 Verification and Application

5.1 Verification

The BEM code is required to be verified on the cases whose analytic solutions are available. The same could also be compared with the commercial codes available with ease in changes made in boundary conditions, material properties, geometry etc. The parameter like displacement amplitude at a point or for complete surface could be taken as variable for comparison and verification between the methods. A simple example for 3D case time harmonic problem is described below.

A cube of dimensions A cube of dimensions 6m X 6m X 6m is subjected to uniform traction field of 100N/m^2 on to the top surface. The shear tractions on all faces of cube are zero and the normal displacement are constraint on lateral and lower faces. The material is Aluminum whose properties are shown in Table 5.1.

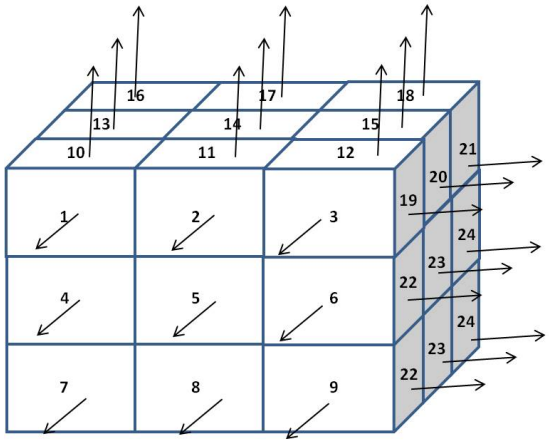

Figure 5.1: Mesh of cube with constant elements having normals pointing outwards

Table 5.1: Aluminum Material Properties

Property	Value	Units
Young's Modulus (E)	70	GPa
Density (ρ)	2700	kg/m^3,
Poisson's ratio (ν)	0.3375	
Shear Modulus (μ)	26.168	GPa

The cube is discretized using constant elements, where the number of nodes are equal to the number of elements. For solving interior elastodynamic problem, the mesh has to performed such that all the normals are always pointing outwards. The use of commercial software Hypermesh gives the preliminary mesh with mesh on boundary with linear quad elements. The available coordinates of nodes are used to obtain the midpoint of each element accounting as the node of the constant element.

The Finite Element Method -ANSYS is used to solve the above problem with same material and geometrical parameters. The discretization of complete domain is done using SOLID 45 which has 8 nodes with each node having three degree of freedom i.e. translations in three coordinate directions. The used mesh in ANSYS contains 6 elements on every edge of the cube, resulting in total number of elements as 216. Also need to take care here about the frequencies being used in code. Throughout BEM code angular circular frequency (ω) is used, where as ANSYS gives results with respect to frequency. Hence for comparison, BEM results are plotted over actual frequency range and not circular frequency.

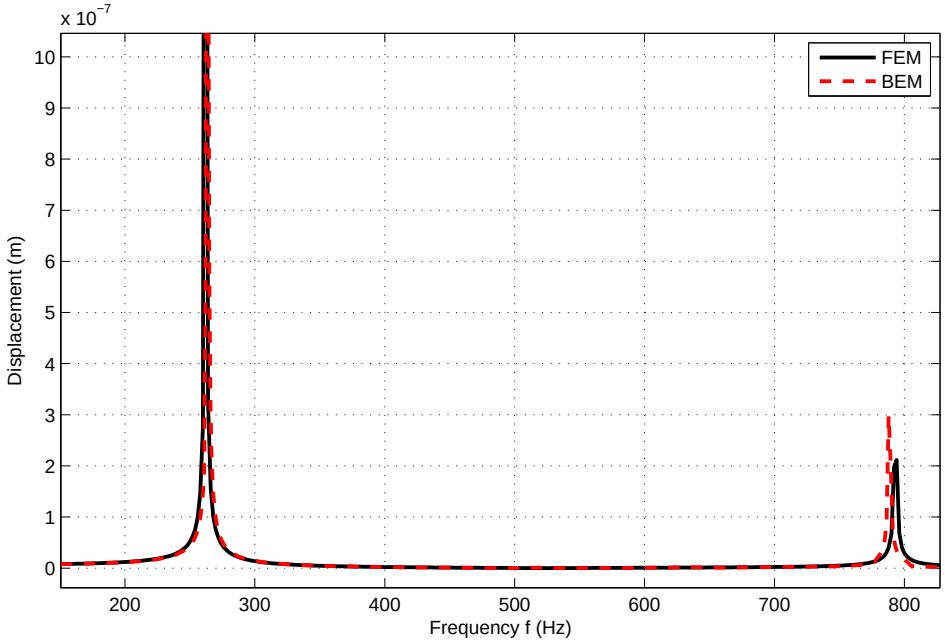

Figure 5.2: Amplitude of displacement at center of upper surface vs frequency

The results of both BEM code and FEM using Ansys have been plotted in figure 5.2 for the displacement at the center node of the upper surface under uniform traction. It could be seen that the results are very close, but for higher frequency there is a slight difference.

The same could be verified for the displacement over the whole upper surface, monitoring the displacement of each node. The boundary conditions shows that theoretically all the upper surface nodes should undergo same displacement, which are satisfied in both FEM and BEM code.

The analytical resonance frequency for above problem is obtained by;

$$\omega = \frac{(2n-1)\pi\ C_p}{2L} \tag{5.1}$$

where, $n = 1, 2....$ are the respective eigen frequencies. Hence, the first and third eigen frequencies for above problem are 261.91 and 785.74 Hz. These values obtained in figure are very close to the analytic solutions. Although for higher frequencies, re meshing is required to satisfy the thumb rule to have more accurate representation of wave propagation

$$max(x_1, x_2) \leq \frac{\lambda_{min}}{10}. \tag{5.2}$$

where, x_1, x_2 represent the edge lengths of the element.

5.2 Modal Decomposition Method

The modal decomposition method is used for the determination of reflection coefficients and transmission coefficients in structures. The method is suitable only for vertical cracks. The coefficients are calculated such that both the continuity and boundary conditions are fulfilled. The waves which are reflected at the discontinuities not only carry the information about the position of the crack but also the geometry (usually measured in depth of crack). A schematic diagram of same could be seen figure 5.3.

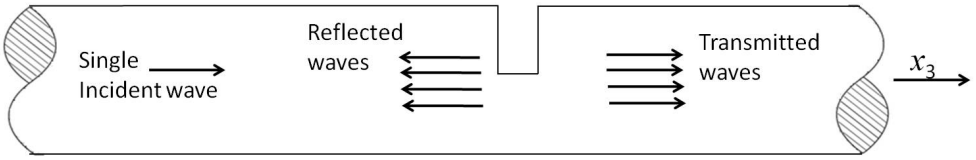

Figure 5.3: Mode conversion at crack section in x_3 direction of propagation

The incident wave would be partially reflected and transmitted. The time harmonic wave propagation representation for displacement field of the incident, reflected and transmitted mode is presented below

$$\begin{aligned} \boldsymbol{u}_{\text{inc}} &= \alpha\ \hat{\boldsymbol{u}}_{\text{inc}}\ e^{ik_{\text{inc}}x_3} \\ \boldsymbol{u}_{\text{refl}} &= \sum_{j=1}^{N} \beta^j\ \hat{\boldsymbol{u}}^j\ e^{ik^j x_3} \\ \boldsymbol{u}_{\text{trans}} &= \sum_{j=1}^{N} \gamma^j\ \hat{\boldsymbol{u}}^j\ e^{ik^j x_3} \end{aligned} \tag{5.3}$$

where, $\boldsymbol{u}_{\text{inc}}$, $\boldsymbol{u}_{\text{refl}}$, $\boldsymbol{u}_{\text{trans}}$ are the displacement field associated with the incident, reflected and transmitted propagating waves. All the reflected and transmitted

waves form the respective fields, which contains both the propagating and evanescent waves. The superposition of the wave fields allow us to define the reflection $\boldsymbol{R}$ and transmission coefficients $\boldsymbol{T}$,

$$\boldsymbol{R} = \frac{\boldsymbol{\beta}}{\alpha} \quad ; \quad \boldsymbol{T} = \frac{\boldsymbol{\gamma}}{\alpha}. \tag{5.4}$$

For a free edge surface there are no transmission of waves, hence only the superposition of incident and reflected wave fields for both displacements and tractions could be said as

$$\begin{aligned} \boldsymbol{u} &= \hat{\boldsymbol{u}}_{\text{inc}} e^{-ik_{\text{inc}}x_3} + \sum_{j=1}^{N} \beta^j \hat{\boldsymbol{u}}^j e^{ik^j x_3} \\ \boldsymbol{t} &= \hat{\boldsymbol{t}}_{\text{inc}} e^{-ik_{\text{inc}}x_3} + \sum_{j=1}^{N} \beta^j \hat{\boldsymbol{t}}^j e^{ik^j x_3} \end{aligned} \tag{5.5}$$

Following the boundary conditions at the free edge $x_3 = 0$,

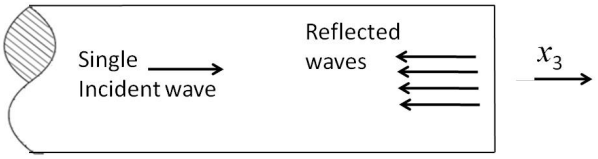

Figure 5.4: Reflected waves from free edge

$$\boldsymbol{t}_{|x_3=0} = \hat{\boldsymbol{t}}_{\text{inc}} + \sum_{j=1}^{N} \beta^j \hat{\boldsymbol{t}}^j = 0 \tag{5.6}$$

Rewriting the above in matrix notation,

$$\boldsymbol{t}_{\text{inc}} + \boldsymbol{T}_{\text{refl}} \boldsymbol{\beta} = 0 \tag{5.7}$$

Least square solution minimizes of the residual surface traction and used to calculate $\boldsymbol{\beta}$ could be obtained from above as

$$\boldsymbol{\beta} = -(\boldsymbol{T}_{\text{refl}}^H \boldsymbol{T}_{\text{refl}})^{-1} \boldsymbol{T}_{\text{refl}}^H \boldsymbol{t}_{\text{inc}} \tag{5.8}$$

The above holds true for the conservation of energy, with the total power of reflected wave equal to the total power of incident wave.

5.3 BE Model

Boundary element method is used at the regions near the free edge. The region near free edge is discretized using surface constant elements. From previous

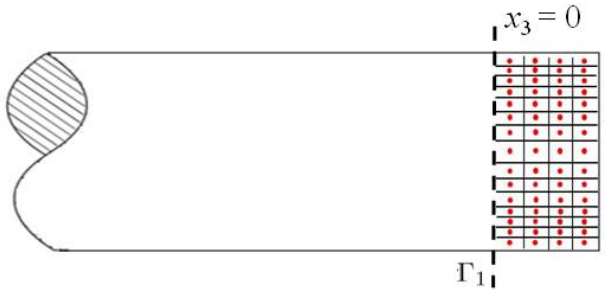

Figure 5.5: BE Model with constant quad elements near free edge

section we could write directly the displacement and traction fields at cross-section Γ_1 as the superposition of incident waves and all possible reflected waves from free edge times their amplitudes.

$$\boldsymbol{u}_{\Gamma_1} = \boldsymbol{u}_{\text{inc}} + \boldsymbol{U}_{\text{refl}}\boldsymbol{\beta} \tag{5.9}$$

$$\boldsymbol{t}_{\Gamma_1} = \boldsymbol{t}_{\text{inc}} + \boldsymbol{T}_{\text{refl}}\boldsymbol{\beta} \tag{5.10}$$

The above equations are represented in matrix form with k number of nodal points used to discretize the near free edge region using constant elements.

$$[\ \boldsymbol{u}_{\Gamma_1}\ ]_{3k\times 1} = [\ \boldsymbol{u}_{\text{inc}}\ ]_{3k\times 1} + [\ \boldsymbol{U}_{\text{refl}}\ ]_{3k\times N}\ [\ \boldsymbol{\beta}\ ]_{N\times 1} \tag{5.11}$$

$$[\ \boldsymbol{t}_{\Gamma_1}\ ]_{3k\times 1} = [\ \boldsymbol{t}_{\text{inc}}\ ]_{3k\times 1} + [\ \boldsymbol{T}_{\text{refl}}\ ]_{3k\times N}\ [\ \boldsymbol{\beta}\ ]_{N\times 1} \tag{5.12}$$

on Γ_1, where

$$\boldsymbol{u}_{\text{inc}} = \begin{bmatrix} \overline{u}_{x_1}(x_3^1) \\ \overline{u}_{x_2}(x_3^1) \\ \overline{u}_{x_3}(x_3^1) \\ \overline{u}_{x_1}(x_3^2) \\ \vdots \\ \vdots \\ \vdots \\ \overline{u}_{x_1}(x_3^k) \\ \overline{u}_{x_2}(x_3^k) \\ \overline{u}_{x_3}(x_3^k) \end{bmatrix} \qquad \boldsymbol{t}_{\text{inc}} = \begin{bmatrix} \overline{t}_{x_1}(x_3^1) \\ \overline{t}_{x_2}(x_3^1) \\ \overline{t}_{x_3}(x_3^1) \\ \overline{t}_{x_1}(x_3^2) \\ \vdots \\ \vdots \\ \vdots \\ \overline{t}_{x_1}(x_3^k) \\ \overline{t}_{x_2}(x_3^k) \\ \overline{t}_{x_3}(x_3^k) \end{bmatrix} \tag{5.13}$$

$$\boldsymbol{U}_{\text{refl}} = \begin{bmatrix} \overline{u}^1_{x_1}(x^1_3) & \overline{u}^2_{x_1}(x^1_3) & \dots & \overline{u}^j_{x_1}(x^1_3) & \dots & \dots & \overline{u}^{N-1}_{x_1}(x^1_3) & \overline{u}^N_{x_1}(x^1_3) \\ \overline{u}^1_{x_2}(x^1_3) & \overline{u}^2_{x_2}(x^1_3) & \dots & \overline{u}^j_{x_2}(x^1_3) & \dots & \dots & \overline{u}^{N-1}_{x_2}(x^1_3) & \overline{u}^N_{x_2}(x^1_3) \\ \overline{u}^1_{x_3}(x^1_3) & \overline{u}^2_{x_3}(x^2_3) & \dots & \overline{u}^j_{x_3}(x^1_3) & \dots & \dots & \overline{u}^{N-1}_{x_3}(x^1_3) & \overline{u}^N_{x_3}(x^1_3) \\ \overline{u}^1_{x_1}(x^2_3) & \overline{u}^2_{x_1}(x^2_3) & \dots & \overline{u}^j_{x_1}(x^2_3) & \dots & \dots & \overline{u}^{N-1}_{x_1}(x^2_3) & \overline{u}^N_{x_1}(x^2_3) \\ \vdots & \vdots & \vdots & \vdots & \dots & \dots & \vdots & \vdots \\ \vdots & \vdots & \vdots & \vdots & \ddots & & \vdots & \vdots \\ \vdots & \vdots & \vdots & \vdots & & \ddots & \vdots & \vdots \\ \overline{u}^1_{x_1}(x^k_3) & \overline{u}^2_{x_1}(x^k_3) & \dots & \overline{u}^N_{x_1}(x^k_3) & \dots & \dots & \overline{u}^{N-1}_{x_1}(x^k_3) & \overline{u}^N_{x_1}(x^k_3) \\ \overline{u}^1_{x_2}(x^k_3) & \overline{u}^2_{x_2}(x^k_3) & \dots & \overline{u}^N_{x_2}(x^k_3) & \dots & \dots & \overline{u}^{N-1}_{x_2}(x^k_3) & \overline{u}^N_{x_2}(x^k_3) \\ \overline{u}^1_{x_3}(x^k_3) & \overline{u}^2_{x_2}(x^k_3) & \dots & \overline{u}^N_{x_3}(x^k_3) & \dots & \dots & \overline{u}^{N-1}_{x_3}(x^k_3) & \overline{u}^N_{x_3}(x^k_3) \end{bmatrix} \tag{5.14}$$

$$\boldsymbol{T}_{\text{refl}} = \begin{bmatrix} \bar{t}^1_{x_1}(x^1_3) & \bar{t}^2_{x_1}(x^1_3) & \dots & \bar{t}^j_{x_1}(x^1_3) & \dots & \dots & \bar{t}^{N-1}_{x_1}(x^1_3) & \bar{t}^N_{x_1}(x^1_3) \\ \bar{t}^1_{x_2}(x^1_3) & \bar{t}^2_{x_2}(x^1_3) & \dots & \bar{t}^j_{x_2}(x^1_3) & \dots & \dots & \bar{t}^{N-1}_{x_2}(x^1_3) & \bar{t}^N_{x_2}(x^1_3) \\ \bar{t}^1_{x_3}(x^1_3) & \bar{t}^2_{x_3}(x^2_3) & \dots & \bar{t}^j_{x_3}(x^1_3) & \dots & \dots & \bar{t}^{N-1}_{x_3}(x^1_3) & \bar{t}^N_{x_3}(x^1_3) \\ \bar{t}^1_{x_1}(x^2_3) & \bar{t}^2_{x_1}(x^2_3) & \dots & \bar{t}^j_{x_1}(x^2_3) & \dots & \dots & \bar{t}^{N-1}_{x_1}(x^2_3) & \bar{t}^N_{x_1}(x^2_3) \\ \vdots & \vdots & \vdots & \vdots & \dots & \dots & \vdots & \vdots \\ \vdots & \vdots & \vdots & \vdots & \ddots & & \vdots & \vdots \\ \vdots & \vdots & \vdots & \vdots & & \ddots & \vdots & \vdots \\ \bar{t}^1_{x_1}(x^k_3) & \bar{t}^2_{x_1}(x^k_3) & \dots & \bar{t}^N_{x_1}(x^k_3) & \dots & \dots & \bar{t}^{N-1}_{x_1}(x^k_3) & \bar{t}^N_{x_1}(x^k_3) \\ \bar{t}^1_{x_2}(x^k_3) & \bar{t}^2_{x_2}(x^k_3) & \dots & \bar{t}^N_{x_2}(x^k_3) & \dots & \dots & \bar{t}^{N-1}_{x_2}(x^k_3) & \bar{t}^N_{x_2}(x^k_3) \\ \bar{t}^1_{x_3}(x^k_3) & \bar{t}^2_{x_2}(x^k_3) & \dots & \bar{t}^N_{x_3}(x^k_3) & \dots & \dots & \bar{t}^{N-1}_{x_3}(x^k_3) & \bar{t}^N_{x_3}(x^k_3) \end{bmatrix} \tag{5.15}$$

As we know from previous section that $\boldsymbol{u}_{\text{inc}}$, $\boldsymbol{t}_{\text{inc}}$, $\boldsymbol{U}_{\text{refl}}$ and $\boldsymbol{T}_{\text{refl}}$ are known from Waveguide-FE method, but the unknowns $\boldsymbol{u}_{\Gamma_1}$, $\boldsymbol{t}_{\Gamma_1}$ and $\boldsymbol{\beta}$ are more than the equations available. The BE model will give us a relation between the unknown displacement and traction field variables on complete boundary of the BE model, and hence at cross-section Γ_1.

$$\boldsymbol{Hu} = \boldsymbol{Gt} \tag{5.16}$$

where, $\boldsymbol{u}$ and $\boldsymbol{t}$ contains the displacement filed and traction fields of all the nodes respectively. The system of equation could be split as

$$\begin{bmatrix} \boldsymbol{H}_{11} & \boldsymbol{H}_{12} \\ \boldsymbol{H}_{21} & \boldsymbol{H}_{22} \end{bmatrix} \begin{bmatrix} \boldsymbol{u}_{\Gamma_1} \\ \boldsymbol{u}_{\Gamma-\Gamma_1} \end{bmatrix} = \begin{bmatrix} \boldsymbol{G}_{11} & \boldsymbol{G}_{12} \\ \boldsymbol{G}_{21} & \boldsymbol{G}_{22} \end{bmatrix} \begin{bmatrix} \boldsymbol{t}_{\Gamma_1} \\ \boldsymbol{t}_{\Gamma-\Gamma_1} \end{bmatrix} \tag{5.17}$$

where, $\Gamma - \Gamma_1$ represent the surface which has known traction boundary conditions. In above system, the known traction boundary conditions could be induced to eliminate the unknown displacement field on $\Gamma - \Gamma_1$. For our case, $\Gamma - \Gamma_1$ is traction free and hence $\boldsymbol{t}_{\Gamma-\Gamma_1} = 0$ This reduces the system of equations to,

$$\begin{bmatrix} \boldsymbol{H}_{11} & \boldsymbol{H}_{12} \\ \boldsymbol{H}_{21} & \boldsymbol{H}_{22} \end{bmatrix} \begin{bmatrix} \boldsymbol{u}_{\Gamma_1} \\ \boldsymbol{u}_{\Gamma-\Gamma_1} \end{bmatrix} = \begin{bmatrix} \boldsymbol{G}_{11} \\ \boldsymbol{G}_{21} \end{bmatrix} \begin{bmatrix} \boldsymbol{t}_{\Gamma_1} \end{bmatrix} \tag{5.18}$$

The system of equation now have only two variable vectors $\boldsymbol{u}_{\Gamma-\Gamma_1}$ and $\boldsymbol{\beta}$ present in terms associated with Γ_1, which could be solved by static condensation.

$$\boldsymbol{u}_{\Gamma-\Gamma_1} = -\boldsymbol{H}_{22}^{-1}\ [\ \boldsymbol{H}_{21}\boldsymbol{u}_{\Gamma_1} - \boldsymbol{G}_{21}\boldsymbol{t}_{\Gamma_1}] \tag{5.19}$$

replacing back into equation

$$[\boldsymbol{H}_{11} - \boldsymbol{H}_{12}\ \boldsymbol{H}_{22}^{-1}\ \boldsymbol{H}_{21}]\boldsymbol{u}_{\Gamma_1} = [-\boldsymbol{H}_{12}\ \boldsymbol{H}_{22}^{-1}\ \boldsymbol{G}_{21}\ ]\ \boldsymbol{t}_{\Gamma_1} \tag{5.20}$$

$$[\boldsymbol{H}_{11} - \boldsymbol{H}_{12}\ \boldsymbol{H}_{22}^{-1}\ \boldsymbol{H}_{21}]\ [\boldsymbol{u}_{\text{inc}} + \boldsymbol{U}_{\text{refl}}\boldsymbol{\beta}] = [\boldsymbol{G}_{11} - \boldsymbol{H}_{12}\ \boldsymbol{H}_{22}^{-1}\ \boldsymbol{G}_{21}\ ]\ [\boldsymbol{t}_{\text{inc}} + \boldsymbol{T}_{\text{refl}}\boldsymbol{\beta}] \tag{5.21}$$

The above equations can be solved for unknown $\boldsymbol{\beta}$ by transforming into form $\mathbf{A}\boldsymbol{\beta} = \mathbf{b}$. where,

$$\boldsymbol{A} = \{[\boldsymbol{H}_{11} - \boldsymbol{H}_{12}\ \boldsymbol{H}_{22}^{-1}\ \boldsymbol{H}_{21}]\ \boldsymbol{U}_{\text{refl}}\ -\ [\boldsymbol{G}_{11} - \boldsymbol{H}_{12}\ \boldsymbol{H}_{22}^{-1}\ \boldsymbol{G}_{21}\ ]\ \boldsymbol{T}_{\text{refl}}\}_{3k\times N} \tag{5.22}$$

and

$$\boldsymbol{b} = \{-[\boldsymbol{H}_{11} - \boldsymbol{H}_{12}\ \boldsymbol{H}_{22}^{-1}\ \boldsymbol{H}_{21}]\ \boldsymbol{u}_{\text{inc}}\ +\ [\boldsymbol{G}_{11} - \boldsymbol{H}_{12}\ \boldsymbol{H}_{22}^{-1}\ \boldsymbol{G}_{21}\ ]\ \boldsymbol{t}_{\text{inc}}\}_{3k\times 1} \tag{5.23}$$

As it is evident that $\boldsymbol{A}$ is not square matrix, it is required to convert equation into a form to get unique solution for $\boldsymbol{\beta}$, which is done by taking multiplying both sides by the conjugate transpose of $\boldsymbol{A}$, and hence $\boldsymbol{\beta}$ could be obtained as

$$\boldsymbol{\beta} = (\boldsymbol{A}^H\boldsymbol{A})^{-1}\boldsymbol{A}^H\boldsymbol{b} \tag{5.24}$$

where, $\boldsymbol{A}^H$ represents the conjugate transpose of $\boldsymbol{A}$. The reflection coefficient could be obtained as the ratio of the amplitudes of the reflected waves to the amplitude of incident wave.

$$\mathbf{R}^{jn} = \boldsymbol{\beta}^j/\boldsymbol{\alpha} \tag{5.25}$$

where, $\mathbf{R}$ represents the total reflection coefficients obtained from the incident modes, with each incident mode giving rise to j modes of reflections. for a single incident wave mode, with $\boldsymbol{\alpha} = 1$

$$\mathbf{R} = \boldsymbol{\beta} = (\boldsymbol{A}^H\boldsymbol{A})^{-1}\boldsymbol{A}^H\boldsymbol{b} \tag{5.26}$$

5.3.1 Application

The practical application considered here is of a traction free cylinder with free edge (basis being motivation from high transmission lines). The cylinder specifications are presented below.

$$\begin{aligned} \text{Daiamter} &: 2\ m \\ \text{Length} &: 0.5\ m \\ \text{Material} &: \text{Aluminum} \\ \text{Boundary Conditions} &: \text{lateral and free edge traction free} \end{aligned} \tag{5.27}$$

Although the actual dimensions of cylinder and the frequency range are in millimeters and kHz respectively, but due to numerical considerations associated with the conditioning of the matrices, the dimensions are taken in meters and frequency in Hz. The change in order of dimensions could be justified form the dimensional analysis. Dimensional analysis is based on the fact that a physical law must be independent of the units used to measure the physical variables. The units have only been changed and hence only the changes is in the amplification of the values of displacement and tractions without effect on the changes in the relation between the amplitudes trends with respect to the frequency or frequency times thickness. As could also be observed for the dispersion curve when plotted for wave number versus frequency-thickness, an increase in order of 10^3 in dimensions balanced by order decrease in frequency.

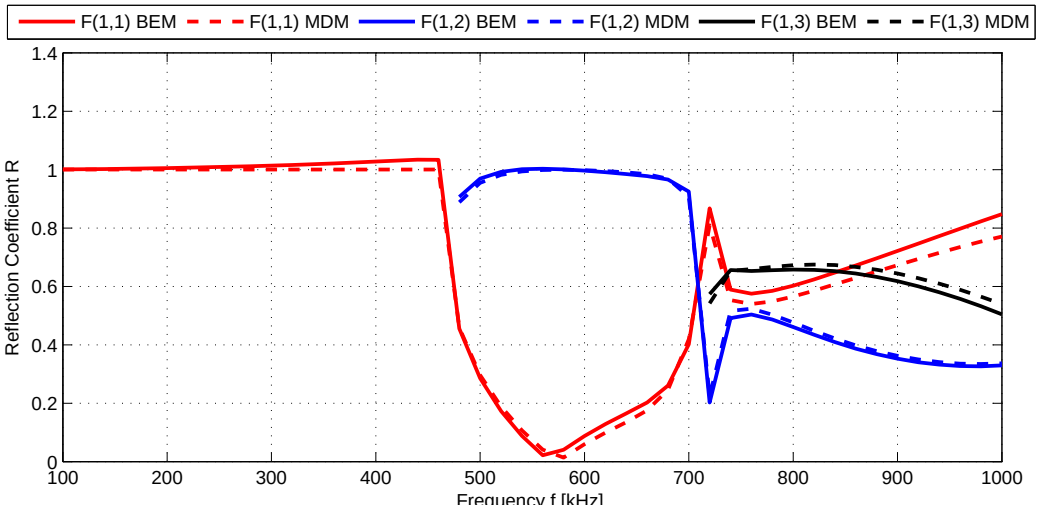

Figure 5.6: Reflection Coeffiecient of reflected waves from free edge of cylinder over a frequency range for incident F(1,1) wave

Figure 5.6 shows the reflection coefficient of the associated reflected waves from free edge of the cylinder due to an incident wave $F(1,1)$. The figure shows a constant reflection coefficient value with single mode $F(1,1)$ propagating wave till small frequency range. With increase in frequency, the propagating modes increases and hence results in more complicated trends for the total reflection coefficient from these propagating modes. The comparison between the FE-Modal decomposition method and BEM values are very close until small frequency ranges, and shows a little variations for increase in frequency where other propagating modes also originate. This could be accounted to relaxation of the discretization criterion, as same mesh being used for all frequencies in BEM analysis. The value of reflection coefficient cannot be more than unity for any single mode in free edge case, as unit reflection coefficent means the complete reflection of incident wave without any mode conversion. The discussion of the same could be elaborated with plotting the energy of the reflected waves over the frequency range.

The conservation of energy principle applicable for free edge ensures that the input energy induced by a single incident mode must be equal to the sum of ener-

gies associated with the multiple reflected modes. Figure 5.7 shows the variation of the energy associated with the reflected modes over the frequency range. With incident wave energy equal to unity, the plot should ideally produce a constant unity value over the complete frequency range to follow energy principle. There a slight variations from the unity value as the frequency increases. The solution from BEM analysis is based on the integral equations and not on virtual work principle, so that the aim was mainly to minimize the residual error and not considering the minimizing the total energy, which results in overshooting of the value above unity also. Other inevitable errors could be associated to approximations in field variables, numerical integration, discretization and finite number of propagating modes used in mode superposition at interface of coupling.

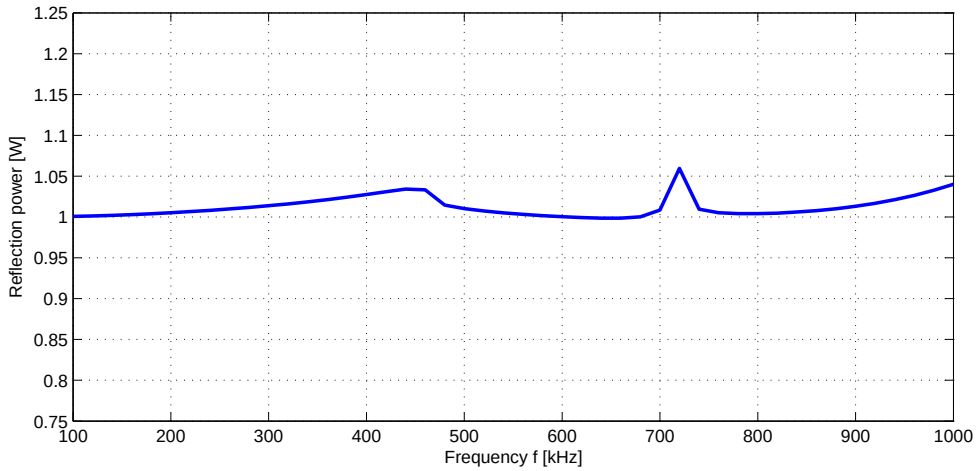

Figure 5.7: Energy associated with the reflected waves from free edge of a cylinder for incident Flexural wave

After observing the solutions for incident Flexural wave F(1,1), the same could be extended to monitor the reflection coefficient plot over a frequency range with single longitudinal wave as incident wave. The portion of the plot at lower frequency is point of concern as the higher frequency tend to show deviation depicted in above application. Figure 5.8 shows the obtained reflection coefficient over frequency range of 100-1000 kHz.

From figure 5.8, it is observed that till frequency of 700 kHz, the reflection coefficient is constant and does not exceed the analytical limiting value of 1. Below frequency level of 600 kHz, there has been no mode conversion and hence all the incident waves are reflected with zero energy loss. But in the range from 600 - 750 kHz, the first mode conversion taking place giving rise to other longitudinal modes, and resulting in start of more complex behavior to monitor. In between 750-800 kHz, there exists an sudden increase in the value of reflection coefficient exceeding the limit value of 1. The similar explanations could be expected as observed in previous case of incident flexural waves.

Also, the plot of the energy associated with the propagating modes being shown

in figure 5.9, where could be observed clearly a constant value till a range with folllowing complete conservation of energy and later on shows deviation with increase in frequency.

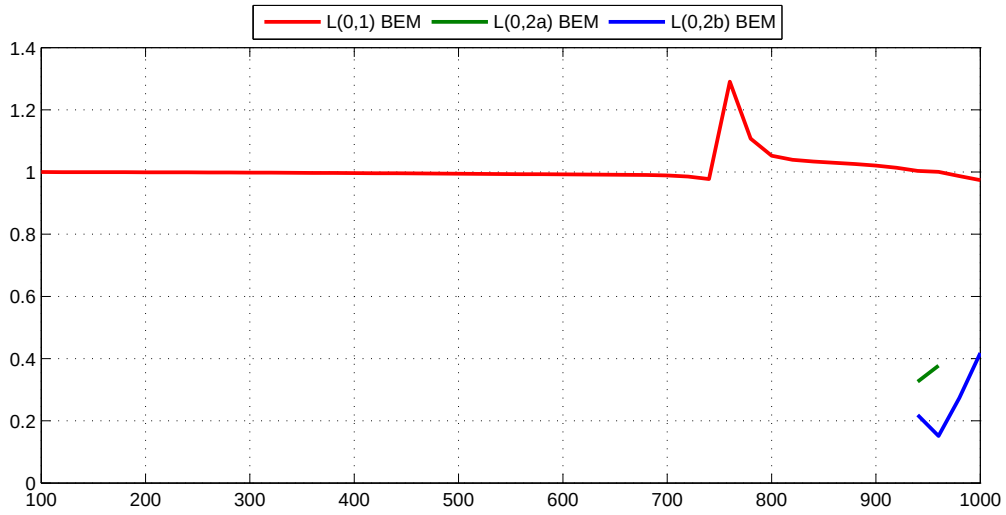

Figure 5.8: Reflection Coefficient of reflected waves from free edge of cylinder over a frequency range for incident L(0,1) wave

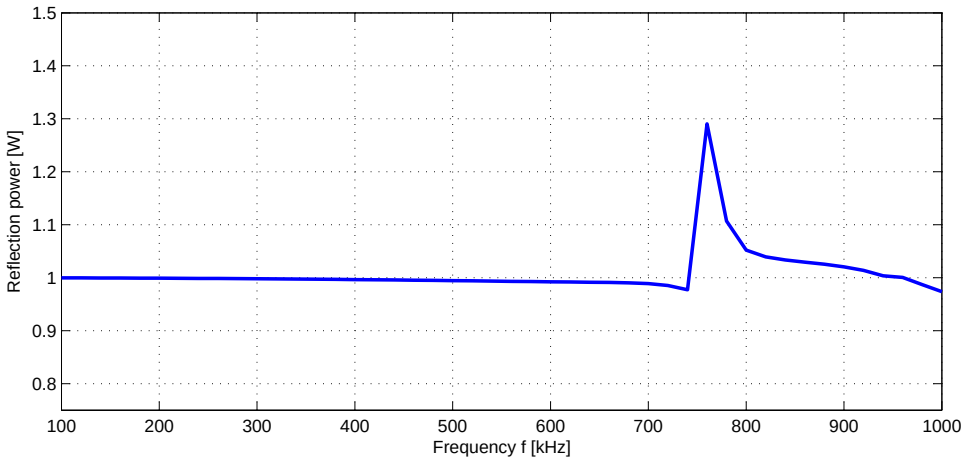

Figure 5.9: Energy associated with the reflected waves from free edge of a cylinder for incident longitudinal wave

6 Experimental Verification

6.1 Experimental Setup

Apart from the numerical solutions with comparison between the conventional FE-Modal decomposition and Boundary Element method, it is also evident to compare the solutions with experimental results for have practice correlation. The experimental setup is shown in figure 6.1.

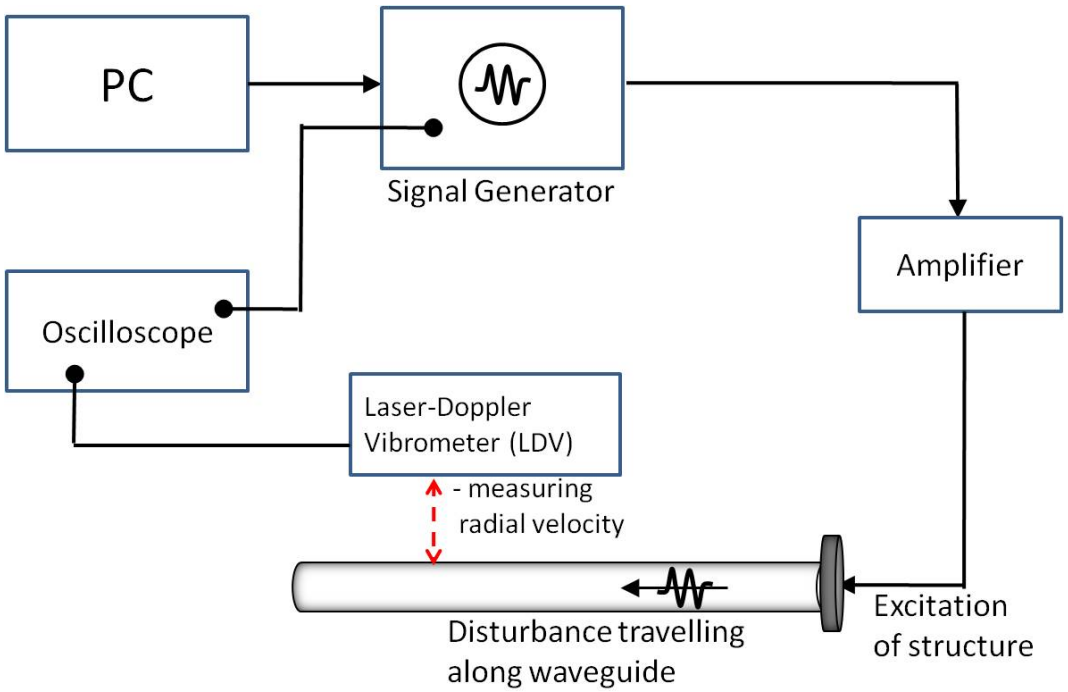

Figure 6.1: Energy associated with the reflected waves from free edge of a cylinder for incident longitudinal wave

The direct output from experimental setup is measured radial velocity components. For this, the Laser Doppler vibrometer (LDV) is placed in such a way that the incident signal is perpendicular to the circumference of the cylinder to measure the radial velocity components as shown in figure 6.2.

The motivation behind selecting points $\boldsymbol{A}$ and $\boldsymbol{B}$ was to differentiate between the traveling longitudinal and flexural wave. As longitudinal waves show uniform radial displacement over any circumferential cross-section. so the velocity measured at points $\boldsymbol{A}$ and $\boldsymbol{B}$ are same for these waves. But there exists two types

of flexural waves, and the radial displacement is not same at points ***A*** and ***B***. Hence, signal correspond to difference between the velocity at points ***A*** and ***B*** representing flexural waves.

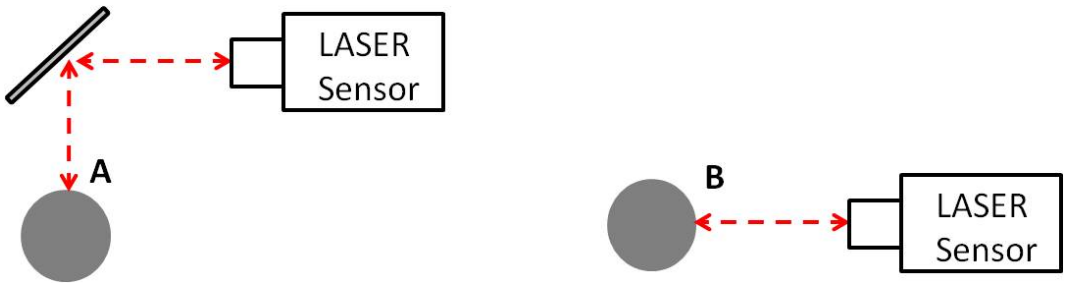

Figure 6.2: Normal velocity components for two types of flexural wave

The process of measurement starts with an excitation of the disturbance from a Piezeo electric transducer. With the help of a signal generator and amplifier, required frequency of excitation with proper strength could be achieved and induced to transducer to transfer the disturbance in the waveguide cylinder. The measurements are taken after a span of time interval, so as allow the disturbance to reach at steady level after reflections from free edge. The LDV sensing unit placed at a distance near the free edge. The sensor's incident waves get reflected from the circumferential surface of the waveguide and means for the measurement of the velocity with which particles vibrate with superposition of reflected waves from free edge. The measured values are made into readable format by using an oscilloscope and thereafter using a code based on modal decomposition method to get the reflection coefficient of the reflected waves form the free edge of the used cylindrical wave guide.

6.2 Results

The longitudinal waves have been point of interest of study for experimental measurements, and hence would look the results corresponding to the same. But to excite only longitudinal wave alone is not possible in practical situations and hence encounter the signals associated with generation and reflections of flexural waves and Torsional waves.

The experiment is performed at 200 KHz, where fundamental L(0,1) and F(1,1) waves exists and torsional waves don't show up due to symmetry. The figure 6.3 shows the signals associated with incident and reflected waves (herein, Longitudinal and Flexural waves) at two points ***A*** and ***B*** as shown in figure 6.2. It could be seen clearly from the plot, that the Longitudinal waves are observed earlier than Flexural waves. This makes task easy for concentration to be focused on Longitudinal waves , as the Flexural waves are not affecting the earlier waves. With each incident wave type, both Longitudinal and Flexural waves are obtained due to reflections from the free edge. The energy associated with the Longitudinal

waves is calculated with known the displacement fields associated with the modes shapes of Longitudinal and Flexural waves. Due to equal radial displacement of Longitudinal waves at the circumference of the cylindrical waveguide, the obtained displacement at points $\boldsymbol{A}$ and $\boldsymbol{B}$ using the results from velocity data of experiments are equal and hence the instantaneous amplitude factor could be obtained as the ratio measured displacement to displacement associated with modal shapes of longitudinal waves.

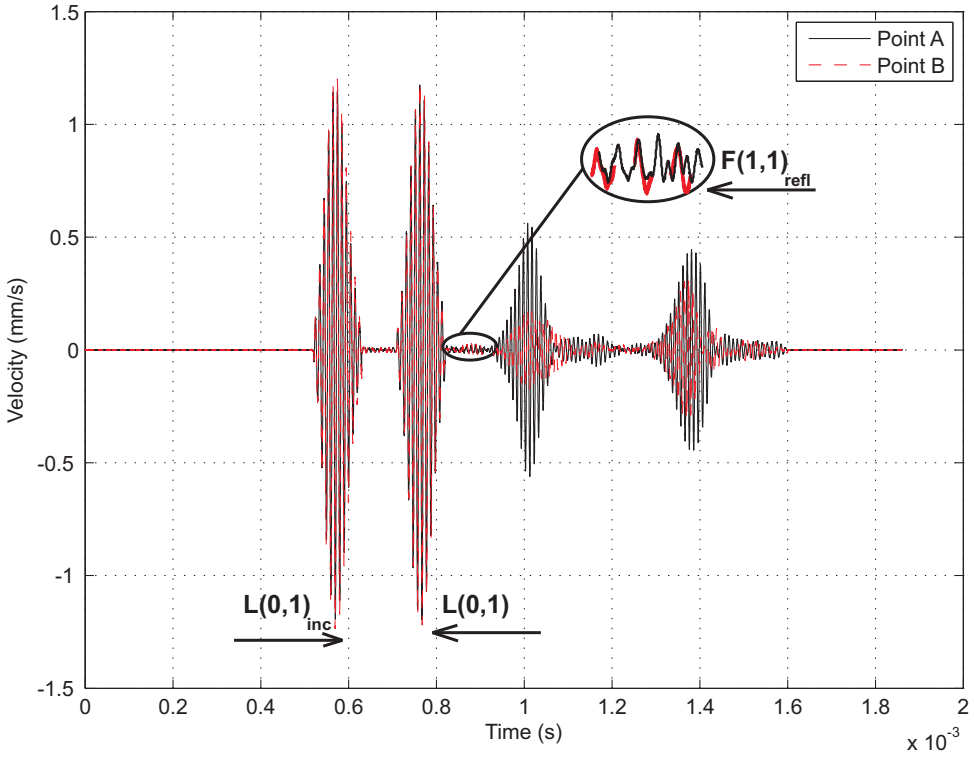

Figure 6.3: Velocity measured at two points for Longitudinal and Flexural waves

$$\hat{\mathbf{a}} = \mathbf{u}_m / \hat{\mathbf{u}}_r \tag{6.1}$$

where, $\hat{\mathbf{a}}, \mathbf{u}_m$ and $\hat{\mathbf{u}}_r$ represents the instantaneous amplitude , measured displacement and modal displacements of longitudinal waves respectively. Modal radial displacement $\hat{\mathbf{u}}_r$ are normalized to have unit average power, such that instantaneous power $\hat{\boldsymbol{P}}$ could be expressed as the root mean square value of the instantaneous amplitude.

$$\hat{\boldsymbol{P}} = 2\hat{\mathbf{a}}^2 \tag{6.2}$$

A time integration over a period duration of the instantaneous power would result in determination of the energy associated with the propagating longitudinal

waves.

$$\boldsymbol{E} = \int_{t_1}^{t_2} \hat{\boldsymbol{P}} dt \tag{6.3}$$

The reflection coefficient from experimental data is calculated using the ratio of the energy associated with Longitudinal reflected waves and incident waves. For the frequency of 200 kHz used in experiments, the calculated reflection coefficient is 1, which coincides with the simulation results shown in figure 5.8.

7 Conclusion and Outlook

From the motivation for detection of discontinuities in cylindrical structures, the Boundary Element method was coupled to the Finite Element- Modal decomposition method to study the mode conversion behavior at the free edge of the waveguide cylinder. The hybrid approach of combining the boundary elements with FE-modal decomposition method is advantageous than conventional approach for various forms of discontinuities. The method has shown good convergence with the results obtained from FE-modal decomposition and experimental methods for range of frequencies at lower regime (around 600 kHz). The complicated behavior with increase in the frequency yielding different modes are not accurately determined but are satisfactory for trend representation. This would require enhancement of discretization with correlation to the frequency change to yield better accurate results. The energy plot has not been convincing for higher frequency regime, where the expected result were to have an unit power from the combined contribution of incident and superimposed reflected waves. The reason associated is the method's dependence on solving boundary integral equation using the collocation method to minimize the residuum than minimizing the energy functional.

The rate at which the results converge has been better due to the use of 2D surface elements than 3D volume elements for discretization at the discontinuous region, herein free edge. Although, this includes the numerical errors associated with interpolation for coupling of surface elements and volume elements with emphasis on the continuity condition at the coupling interface and also increase the computational time.

Although, for lower frequencies being field of interest have shown good results, but the method would require still some improvements to achieve more precise and accurate results for even higher frequencies. The amount of computational time could well be decreased with inclusion of methodology to solve the symmetric model of the cylindrical waveguide structure. This would also evidently decrease the effort and time for interpolation at the coupling of surface elements to volume elements. Also, using Galerkin method, the system of equations involving non symmetric matrices could be transformed into symmetric matrices, so that conventional approaches could be used to solve the systems of equations with ease. Galerkin method gives flexibility in choice of shape function for the primary and secondary variables, where using quadratic elements for displacement fields and constant elements for traction fields would improve the quality of results with less time for computation. The virtual work principle based hybrid displacement or stress boundary element method would work on the minimization

of energy and would satisfy the condition of constant unit power over frequency range. The method could be extended for the applications for studying the mode conversion at discontinuities of any form. The same code would be sufficient to proceed for cracks with inclusion of transmissions factors, while the only changes are made into geometry and hence are changes in $\boldsymbol{H}$ and $\boldsymbol{G}$ matrices. This would be computed at very less time when compared to conventional approach.

Bibliography

[1] J. D. Achenbach. *Wave Propagation in Elastic Solids*. Elsevier, first edition, 1999.

[2] Younho Cho and Joseph L. Rose. A boundary element solution for a mode conversion study on the edge reflection of lamb waves. *Journal of the Acoustical Society of America*, 99:2097–2109, 1996.

[3] J. Dominguez. *Boundary Elements in Dynamics*. Elsevier, 1993.

[4] L. Gaul and C. Fiedler. Improved calculation of filed variables in the domain based on bem. *Engineering Analysis with Boundary Elements*, 93:257–264, 1993.

[5] L. Gaul, M. Koegl, and M. Wagner. *Boundary Element Method for Engineers and Scientists*. Springer, 2003.

[6] K. F. Graff. *Wave Motion in Elastic Solids*. Oxford University Press, 1975.

[7] B. R. Mace, D. Duhamel, M. J. Brennan, and L. Hinke. Finite element prediction of wave motion in structural waveguides. *Journal of the Acoustical Society of America*, 117:2835–2843, 2005.

[8] B. Morvan, N. Wilkie-Chancellier, H. Duflo, A. Tinel, and J. Duclos. Lamb wave reflection at the free edge of a plate. *The Journal of the Acoustical Society of America*, 113:1417–1425, 2003.

[9] Joseph L. Rose. *Ultrasonic Waves in Solid Media*. Cambridge University Press, 1999.

[10] Helge Sprenger. *Modeling, Simulation and Experimental Analysis of Ultrasonic Wave Propagation in Cable with Cracked wires*. Universitaet Stuttgart, 2011.